Atomistic resolution structure and dynamics of lipid bilayers in simulations and experiments ☆

O. H. Samuli Ollila[a,*], Georg Pabst[b,c]

[a] *Department of Neuroscience and Biomedical Engineering, Aalto University*
[b] *University of Graz, Institute of Molecular Biosciences, Biophysics Division, NAWI Graz, Humboldtstr. 50/III, Graz, Austria*
[c] *BioTechMed-Graz, Graz, Austria*

Abstract

Accurate details on the sampled atomistic resolution structures of lipid bilayers can be experimentally obtained by measuring C–H bond order parameters, spin relaxation rates and scattering form factors. These parameters can be also directly calculated from the classical atomistic resolution molecular dynamics simulations (MD) and compared to the experimentally achieved results. This comparison measures the simulation model quality with respect to 'reality'. If agreement is sufficient, the simulation model gives an atomistic structural interpretation of the acquired experimental data. Significant advance of MD models is made by jointly interpreting different experiments using the same structural model. Here we focus on phosphatidylcholine lipid bilayers, which out of all model membranes have been studied mostly by experiments and simulations, leading to the largest available dataset. From the applied comparisons we conclude that the acyl chain region structure and rotational dynamics is generally well described in simulation models. Also changes with temperature, dehydration and cholesterol concentration are qualitatively correctly reproduced. However, the quality of the underlying atomistic resolution structural changes is uncertain. Even worse, when focusing on the lipid bilayer properties at the interfacial region, e.g. glycerol backbone and choline structures, and cation binding, many simulation models produce an inaccurate description of experimental data. Thus extreme care must be applied when simula-

☆ This work is dedicated to the memory of respected colleague and former supervisor, Dr. Marja Hyvönen.

* Corresponding author
Email address: samuli.ollila@aalto.fi (O. H. Samuli Ollila)

tions are applied to understand phenomena where the interfacial region plays a significant role. This work is done by the NMRlipids Open Collaboration project running at `nmrlipids.blogspot.fi` and `https://github.com/NMRLipids`.

Keywords: phosphatidylcholine, NMR, x-ray scattering, neutron scattering, form factor, order parameter

---

1. Introduction

Atomistic resolution structure and dynamics of lipid bilayers have been studied with wide range of techniques for many decades motivated mainly by their presence and important role in biological systems [1, 2, 3, 4, 5, 6, 7]. Lipid bilayers play direct or indirect role in several physiological and pathological molecular scale processes [8, 9, 10, 11]. To fully understand these processes the atomistic and molecular level understanding of lipids is required. Since atomistic resolution studies are extremely difficult for biological membranes, simplified lipid-only systems are often used [1, 2, 3, 4, 5, 6, 7]. The biological relevance of these model systems is supported, e.g. by similar NMR order parameters measured from living cells, lipid extracts and model systems [12, 3, 13].

The most detailed information about lipid bilayer atomistic resolution structure and dynamics has been achieved with various Nuclear Magnetic Resonance (NMR) and scattering techniques [1, 3, 4, 5, 6, 14, 15, 16]. The first one giving direct information on structures sampled by individual lipid molecules [1, 3, 4, 5] and the latter one giving complementary information on average bilayer properties, like e.g. area per lipid or bilayer thickness [6, 14, 15, 16]. Both techniques give robust, accurate and reproducible quantities related to the structure and dynamics. However, for structural and dynamical interpretation both techniques needs a model reproducing the measured quantities [3, 4, 5, 6, 14, 15, 16].

On the other hand, remarkable progress in hardware and software allows to routinely perform classical atomistic resolution molecular dynamics (MD) simulations of lipid bilayer with duration of tens or hundreds nanoseconds. Ideally the molecules are sampling realistic conformations with realistic speed in these simulations. This can

be verified by calculating directly measurable quantities from simulations and comparing these to experimental values. Here we review such comparisons for different experimental observables: C–H bond order parameters, spin relaxation times and form factor. The first and second parameters are measured with NMR. Hence, they represent the structure and dynamics sampled by individual lipid molecules, respectively. The third quantity is obtained from elastic X-ray or neutron scattering experiments and encodes the overall structural bilayer properties.

The order parameters and spin lattice relaxation times have been compared between simulations and experiments for validation and interpretation since the early days of lipid MD simulations [17, 18]. On the other hand, scattering form factors for lipid bilayers have been replacing the comparisons of simulations to the experimental area per molecule during the last decade since form factors are directly measurable quantities while values for area per molecule value depend on specific models used to analyze the scattering data [6].

If an atomistic resolution model reproduces all the above mentioned experimental parameters, i.e. order parameters, spin relaxation rates and form factor, the simulation can be considered as an ultimate model giving interpretation for all these experiments simultaneously. In addition, it would be the correct atomistic resolution representation of the system with high probability since it reproduces large amount of independently measured experimental parameters simultaneously. Thus, the usage of the model for further specific questions and applications would be well justified.

Here we discuss comparisons of order parameters, spin relaxation rates and scattering form factors between simulations and experiments in order to quantify the simulation model quality and interpret the experiments. Also related technical details on experimental data and simulation analysis are discussed. We focus on phosphatidylcholine lipid bilayers due to most comprehensive available datasets for both, simulations and experiments. However, the basic ideas of the approach is valid also for other molecules [19, 20, 21, 22, 23, 24, 25, 26]. We pay special attention on the accuracy and applications of the NMR order parameter data for the glycerol backbone and choline which is often overlooked in the literature. Changes in lipid bilayer properties with varying conditions and the relation to, e.g. ion partition are also discussed.

The general conclusion is that the hydrophobic acyl chain region is well described in simulation models, thus the simulations can considered as the state of the art model with atomistic resolution for this region. However, the glycerol backbone and choline regions are less well described in simulation models, thus extreme care must be taken when phenomena related to the interfacial region are studied with simulations. Due to the large variation of lipid headgroups present in biological systems, the chemical and structural details of the interfacial region are expected to be relevant in several biochemical processes. For example, cell membrane interactions with ions, drug molecules and proteins may be regulated by these details. Here we demonstrate how atomistic resolution model quality can be estimated to minimize potential artificial conclusions produced by simulations.

2. C-H bond order parameters as atomistic resolution structural measure

2.1. Definition and properties of C-H bond order parameter

In lipid bilayer systems the order parameter of a hydrocarbon C–H vector is typically defined as

$$S_{\mathrm{CH}} = \frac{1}{2}\langle 3\cos^2\theta - 1\rangle, \tag{1}$$

where the angle brackets denote an ensemble average over the sampled conformations, and θ is the angle between the C–H bond and the membrane normal. The numerical values of order parameters vary between $-\frac{1}{2} < S_{\mathrm{CH}} < +1$ depending on the sampled θ distribution. The definition is motivated by its connection to the dipolar and quadrupolar splitting measured with ^{1}H-^{13}C NMR and ^{2}H NMR techniques, respectively. The functional form comes from the fundamental theory of interactions between spin systems which gives a connection between average molecules orientations and NMR measurables [27].

If the sampled distribution of θ for a C–H bond are known, the order parameter can be straightforwardly calculated from Eq. 1. However, the sampled θ distributions cannot be uniquely determined from the known order parameter. Thus the experimental order parameter values gives a set of conditions which the structural molecular model

(more specifically the C–H bond vectors of the model) has to fulfill, but the experimental order parameters alone cannot be used to uniquely resolve the structure. The same applies practically to all experimental parameters used in biomolecular structure determination.

Atomistic resolution molecular dynamic simulations naturally produces the sampled structures and the calculated θ distributions can be substituted into Eq. 1 to calculate the order parameters. If and only if the experimental order parameters are reproduced, the sampled structures can be considered as a realistic atomistic resolution representation and used to interpret experimental order parameters. Before MD simulations were feasible for such usage, other models have been used for this interpretation [28, 29, 30, 31, 3, 4, 5, 32, 33, 34, 35]. It is important to note, however, that reproduction of the order parameters does not absolutely guarantee that the sampled structures are correct since several structural models can produce the same order parameters, in principle. Significant advance of the MD models compared to the traditional models is that the same MD structures can be straightforwardly compared to other experimental observables in addition to order parameters, like ^{31}P chemical shift anisotropy [36], ^{31}P-^{13}C dipolar couplings [37], spin relaxation data [38] and scattering data [39]. The comparisons of the same model to the various independently measured experimental observables significantly reduces the possibility of getting unrealistic structures.

The probability for unrealistic structures is further reduced by the large amount of experimentally available order parameter values. As discussed in this review, the order parameters can be measured with high accuracy for each C–H pair of a lipid molecule in a liquid crystalline bilayer [1, 3, 4, 40, 41, 42, 43]. Also the signs [44, 34, 40] and stereospecificity of C–H segments in the same carbon (*forking*) [45, 12, 46, 40, 41, 42] are experimentally available. Consequently, a realistic atomistic resolution model, for example, for POPC molecule (see Fig. 1 B)) in liquid crystalline bilayer has to reproduce 82 experimental order parameter values. If these parameters are not reproduced for certain segments, the model deficiencies are easy to localize since the segmental order parameter is a very local quantity depending only on the position of two atoms (C-H pair). This is an advance over several other accurately measured NMR quantities and scattering form factors depending on the position of several atoms [37, 36, 39],

thus complicating the localization of structural differences in the case of disagreement between model and experiments.

Experimental order parameter data for single component lipid bilayers are easily available in the literature [63, 64, 65, 66, 42, 67, 68, 43]. The amount of data, especially from ^{13}C NMR, has been also increasing of late [63, 64, 42, 67, 68]. Further, changes of order parameters for all lipid segments have been measured various experimental different conditions, like temperature [28, 29, 30, 69], hydration level [49, 70, 71, 41] and in the presence of charged objects [48, 72, 73, 74], cholesterol [75, 69, 42, 68] and proteins [76, 77, 67]. Since the comparison of order parameter responses between experiments and simulations has not been much utilized, we will exemplify its potential by showing the effect of Na^+ ions on choline order parameters and its relation to ion partition in simulations [78] and experiments [48, 72, 73, 74].

In this work we discuss only order parameters obtained from multilamellar samples, as they are the closest experimental analogue to MD simulations with periodic boundary conditions. We do not discuss order parameters measured for other type of samples, such as bicelles [79, 80, 81], or indirect measurements by using, e.g. relaxation data [82] since the comparison to the standard simulation setup is less straightforward.

2.2. Order parameters from ^{2}H NMR experiments

The absolute values of order parameters are connected to the quadrupolar splitting $\Delta\nu_Q$ in ^{2}H NMR experiments through the equation

$$|S_{\mathrm{CD}}| = \frac{4}{3}\frac{h}{e^2qQ}\Delta\nu_{\mathrm{Q}}, \tag{2}$$

where e is the elementary charge, Q is the deuteron quadrupole moment and h is the Planck's constant. The parameter q is related to the largest electric field gradient and in practise its value is not known; therefore the static quadrupolar coupling constant $\frac{e^2qQ}{h}$ is defined, and its value is measured for different compounds in their solid state ($\Delta\nu_Q$ measurement from the system where order parameter is known to be 1). The value measured for different alkenes, $\frac{e^2qQ}{h}$=170 kHz is typically used in C-D order param-

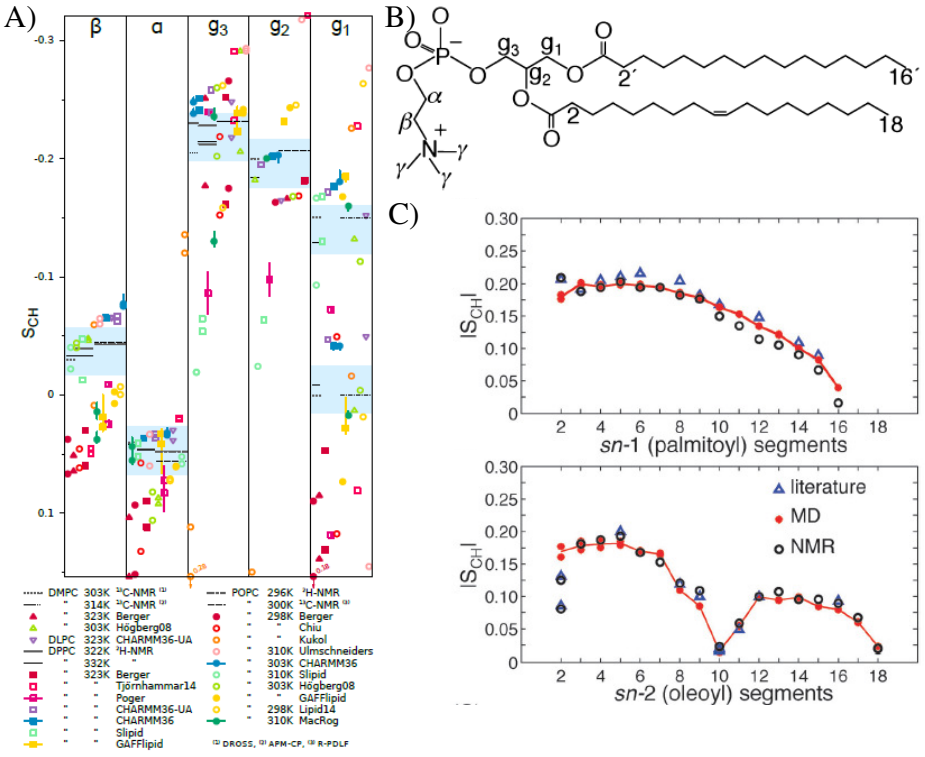

Figure 1: A) Order parameters from simulations and experiments for phosphatidylcholine headgroup and glycerol backbone segments [43]. The blue shaded regions show the subjective sweetspots where the simulation data should fall to agree with experiments, based on estimated quantitative accuracy of order parameter measurements by Botan et al. [43]. Adapted with permission from Botan et al. J. Phys. Chem. B. **2015**, 119, 15075-15088 Copyright 2015 American Chemical Society. B) Chemical structure of 1-palmitoyl-2-oleoylphosphatidylcholine (POPC). C) Order parameters $|S_{\mathrm{CH}}|$ for POPC acyl chains from ^{1}H-^{13}C NMR at 300K (black dots) [42], from ^{2}H NMR at 300K (blue triangles, literature) [31, 47] and from MD simulations at 298K (red dots) [42]. Adapted from Ref. [42] with permission from the PCCP Owner Societies. The experimental values shown in A): DMPC 303 K [40], DMPC 314 K [41], DPPC 322 K [29], DPPC 323 K [48], POPC 296 K [49], and POPC 300 K [42]. The force fields in A): Berger [50], Hogberg08 [51], Poger [52], Ulmschneiders [53], Kukol [54], Chiu [55], CHARMM36 [56], GAFFlipid [57], Slipid [58], MacRog [59], Tjörnhammar14 [60], Lipid14 [61], CHARMM36-UA [62]. The interactive version of A) is available at https://plot.ly/∼HubertSantuz/72/lipid-force-field-comparison/.

eter measurements for lipids. The relation between order parameters and quadrupolar splittings then becomes $S_{\mathrm{CD}} = 0.00784 \times \Delta\nu_{\mathrm{Q}}$. With this relation the quadrupolar splittings reported in the literature can be translated to the order parameter values. For a review and more accurate description see, e.g. Ref. [1].

For ^2H NMR measurements the CH_2 segments have to be labeled with deuterium. This can be done specifically for a certain segment or for the several segments simultaneously [4, 5, 65]. In the first case, it is known that the measured order parameter (quadrupolar splitting) is related to the labeled segment. In the latter case several order parameters (quadrupolar splittings) are simultaneously measured which arise from all the labeled segments, however, it is not known which order parameter belongs to which CH_2 segment. Majority of the ^2H NMR data in the literature are measured using samples with perdeuterated acyl chains [65, 66] while also order parameter data from specifically deuterated lipids are available for several lipid types in various conditions [28, 45, 30, 31, 12, 48, 72, 74, 76, 77, 70, 69].

2.3. Order parameters from ^{13}C NMR experiments

The order parameter can be related to the dipolar splitting $\Delta\nu_{\mathrm{CH}}$ from ^{13}C-^{1}H NMR experiment which is related to the effective dipolar coupling d_{CH} through a scaling factor depending on the used pulse sequence [44, 40, 41, 42]. The effective dipolar coupling d_{CH} is then connected to the absolute value of order parameter through equation

$$|S_{\mathrm{CH}}| = (\frac{D_{\mathrm{max}}}{2\pi})^{-1} d_{\mathrm{CH}}, \tag{3}$$

where $D_{\mathrm{max}} = \frac{\hbar\mu_0\gamma_h\gamma_c}{4\pi\langle r^3_{\mathrm{CH}}\rangle}$. r_{CH} is the C-H distance, μ_0 is the vacuum permittivity, and γ_h and γ_c are the gyromagnetic constants for ^{1}H and ^{13}C nuclei. In contrast to Eq. 2, all the parameters in Eq. 3 are in principle known. However, for the internuclear distance only the average $\langle r_{\mathrm{CH}}\rangle$ is known, but not the third moment $\langle r^3_{\mathrm{CH}}\rangle$. For this reason frequencies between 20.2-22.7 kHz have been used for $\frac{D_{\mathrm{max}}}{2\pi}$ [44, 40, 41, 83, 42, 38].

In contrast, specific labeling is not needed for ^{13}C NMR experiments due the natural abundance of ^{13}C. Labeling can be, however, used to enhance the signal for a specific segment of interest [84]. Order parameter measurements with ^{13}C NMR are

2D experiments, the chemical shift being in the first dimension and dipolar coupling in the second [44, 40, 41, 42]. The chemical shift depends on the local chemical environment and is different for each carbon segment. In the second dimension the dipolar coupling (order parameter) corresponding to each chemical shift value is measured, and its value can be connected, in principle, to each carbon segment by using the chemical shift value. This is straightforward for hydrocarbon segments in choline, glycerol backbone, close to the double bonds, and in the beginning and the end of acyl chains due to their distinct chemical shift values [44, 40, 41, 42, 68]. Challenges occur in the acyl chain region, where chemical shift values of different segments are very close to each other [44, 40, 41, 42, 68]. This issue has been solved by filtering the spectra by using partially deuterated lipids and data from simulations to help the assignment [42, 68].

2.4. Quantitative accuracy of experimental order parameter values

It must be stressed that ^{2}H NMR and ^{13}C NMR are fully independent experiments since the deuterium quadrupolar splitting $\Delta\nu_Q$ and the dipolar splitting d_{CH} are different physical observables. In addition, the prefactors connecting the observables to the order parameter (Eqs. 2 and 3) are independently measured. Further independent experiments are performed by measuring the ^{1}H-^{13}C dipolar couplings using different pulse sequences [44, 40, 41, 42] when the connection between dipolar splitting $\Delta\nu_{\mathrm{CH}}$ and effective dipolar coupling d_{CH} is different.

The quadrupole $\Delta\nu_Q$ and dipolar d_{CH} splittings can be measured with higher accuracy than the prefactors connecting them to order parameters in Eqs. 2 and 3, thus in practise the prefactors determine the quantitative accuracy of measured order parameters. Since the prefactors are determined independently in ^{2}H and ^{13}C NMR measurements, the quantitative accuracy is best estimated by comparing the measured order parameter values from different experiments.

These comparisons are done by several authors and generally show a very good agreement [40, 41, 42, 43, 68]. Botan et al. collected literature values for PC lipid choline headgroup and glycerol backbone order parameters and suggested that order parameters are known with the accuracy of ± 0.02 for these segments in purified PC lipid bilayer samples [43] which agrees with the estimate of Gross et al [40]. Based on

this estimation Botan et al. suggested sweet spots where choline and glycerol backbone order parameters from simulations should range, see Fig. 1 A). Also acyl chain order parameters from different techniques are in good agreement when compared by several authors [40, 41, 42, 68], however, the 0.02 accuracy might not be achieved for some segments.The comparison by Ferreira et al. [42] for POPC acyl chains is also shown in Fig. 1 C).

2.5. Qualitative accuracy of experimental order parameter values

When order parameter changes are measured with varying conditions, like temperature [28, 30, 69], hydration level [49, 70, 71, 41], presence of ions [48, 72, 73, 74], cholesterol [75, 69, 42, 68] or proteins [76, 77, 67], the prefactors connecting order parameters and measured couplings in Eqs. 2 and 3 can be considered to be unchanged. Therefore, accuracy of the measured change is determined by the accuracy of the splitting measurement, in contrast to the quantitative accuracy discussed in previous section. Here we refer to this as a qualitative accuracy. Due to the high resolution of splitting measurements, especially in ^{2}H NMR, the qualitative accuracy is much higher than the quantitative accuracy.

The high qualitative accuracy of order parameter measurements is demonstrated in Figs. 2 and 3 showing the measured changes as a function of ion concentrations and hydration level, respectively. Systematically observed order parameter decrease of choline α and β segments due to penetrating positive charges [48, 72, 73, 74] from ^{2}H NMR are shown in Fig. 2 A). The quadrupole splittings reported in the original work [48] and corresponding order parameters are shown. The distinct quadrupolar splitting changes correspond to order parameter changes below 0.03 and 0.05 units for β and α, respectively. Systematically observed increase for choline β and α segments due to decreased hydration level are shown in Fig. 3. A similar increase is observed for different phosphatidylcholine lipids in slightly different temperatures by different groups using both ^{2}H NMR [49, 70] and ^{13}C NMR [85]. The results demonstrate the systematic changes only slightly above 0.01 units can be detected also with ^{13}C NMR [85].

In conclusion, the order parameter changes can be measured with very high ac-

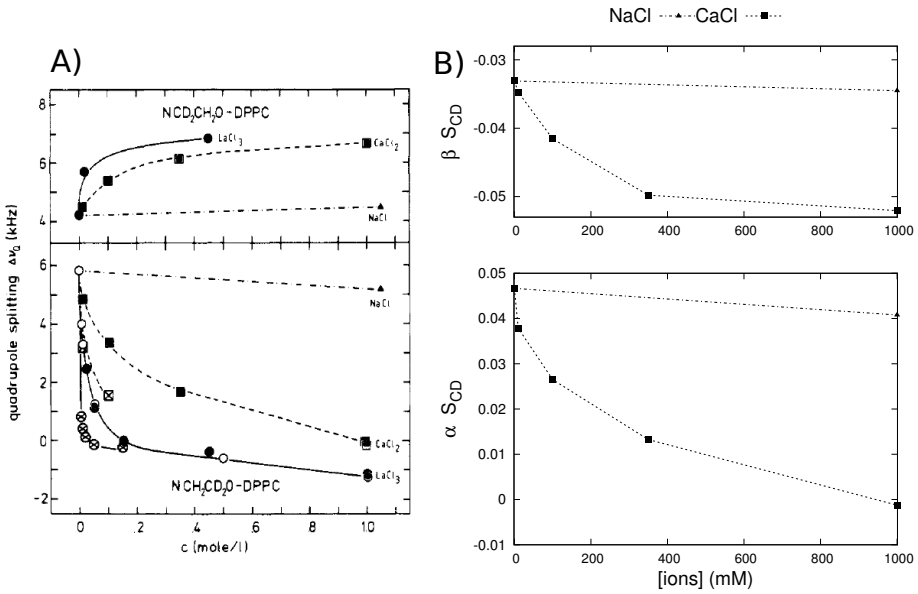

Figure 2: A) Quadrupolar splittings of DPPC α and β segments as a function of different ion concentrations measured by Akutsu and Seelig with ^{2}H NMR [48]. Adapted with permission from Akutsu et al. Biochemistry **1981**, 20, 7366-7373. Copyright 1981 American Chemical Society. B) The measured quadrupolar splittings with NaCl and $CaCl_2$ translated to order parameters ($S_{\mathrm{CD}} = 0.00784 \times \Delta\nu_{\mathrm{Q}}$). The negative sign for β order parameter is assigned according to more recent experiments [44, 34, 40] (see also Ref. [43] and Section 2.6). These changes were later shown to be consistent with the addition of different charges into the bilayer, and the electrometer concept was introduced to measure the amount of charge incorporated in the bilayer interface [48, 72, 73, 74].

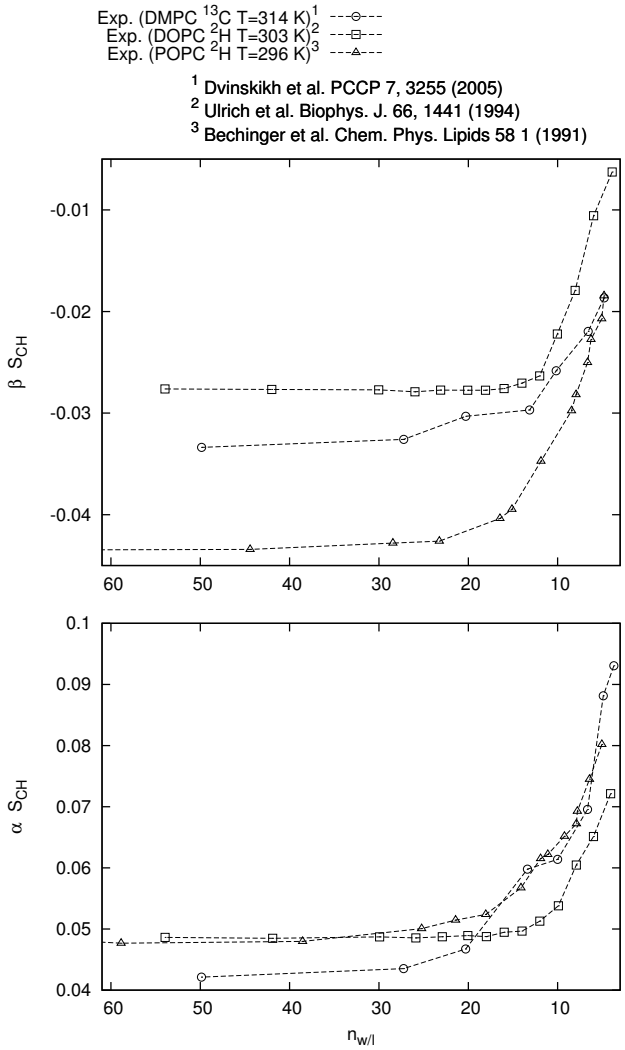

Figure 3: Systematic increase of phosphatidylcholine α and β order parameters with decreasing hydration level, observed with both ^{2}H NMR [49, 70] and ^{13}C NMR [85]. The negative sign for β order parameter is assigned according to more recent experiments [44, 34, 40] (see also Ref. [43] and Section 2.6). The choline order parameter increase is related to the P-N vector tilting more parallel to the membrane plane [43] while relation between order parameter decrease and tilting more perpendicular has been suggested [74].

curacy, thus even very small structural changes can be observed. Molecular models are necessary to analyze the measured changes to avoid over-interpretation of minute changes observed in experiments. For example, high concentration of cholesterol induces measurable changes (less than 2 kHz) to the DPPC α and β quadrupolar splittings, however, the related structural changes are probably almost negligible [75, 43].

2.6. Signs of order parameters

^{2}H NMR [1] and standard ^{1}H-^{13}C NMR [44, 40, 41, 42] measure only the absolute value of order parameter. However, two different ^{1}H-^{13}C NMR techniques applied to eggPC [44] and DMPC [44, 40] allow also the measurement of the sign. The experiments report negative order parameters for almost all the segments, only α and γ are positive. Furthermore, the signs [44, 34, 40] and magnitudes [12, 42, 43] of choline headgroup and glycerol backbone order parameters are practically unaffected by the acyl chain contents of the bilayers. The results indicate that the order parameter signs for these segments can be assumed to be the same in all PC lipids in bilayer. On the other hand, positive signs for g_1, g_3 and C_2 have been reported by Aussenac et al. [79], which has led to some confusion in the simulation community [86, 51, 87]. However, these signs were not directly measured but extracted from the model used to interpret ^{2}H NMR order parameters from DMPC bicelles [79]. Thus, it is reasonable to conclude that order parameters are negative for all segments except for α and γ, as directly measured with ^{1}H-^{13}C NMR [44, 34, 40].

In measurements of order parameter changes with respect to varying conditions [28, 30, 49, 70, 71, 41, 48, 72, 73, 74, 75, 69, 42, 68, 76, 77, 67] only the absolute values are measured. However, the experiments are usually done by gradually changing the conditions and systematic order parameter responses are observed [48, 72, 49, 70, 85, 71, 42] (see also Figs. 2 and 3), indicating that sudden changes of sign do not occur. On the other hand, the large amount of bound positive charge may decrease the α carbon order parameter below zero as demonstrated by the spectra measured by Altenbach and Seelig [72] for POPC with high concentrations of $CaCl_2$, shown in Fig. 4.

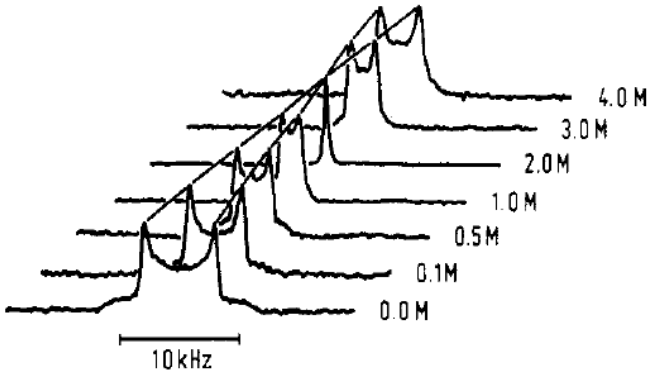

Figure 4: Quadrupolar splitting $\Delta\nu_Q$ for α segment in POPC as a function of $CaCl_2$ concentration measured by Altenbach and Seelig [72] at 313 K. The splitting is related to the order parameter as $S_{\rm CD} = 0.00784 \times \Delta\nu_Q$. More recent studies show that the α order parameter is positive in the absence of $CaCl_2$ [44, 34, 40]. Thus, the most obvious interpretation is that the α order parameter decreases to zero when $CaCl_2$ concentration reaches 2.0M, and becomes increasingly negative with further addition of $CaCl_2$. Reprinted with permission from Altenbach and Seelig, Biochemistry, 23, 3913 (1984). Copyright 1984 American Chemical Society.

2.7. Forking of order parameters

The order parameters for two C–H bonds in the same CH_2 segment are equal for the most lipid segments [28, 30, 31, 12, 40, 41, 42]. Exceptions in a fluid PC lipid bilayer are g_1, g_3, and the C_2 carbon in the *sn*-2 chain segments as observed with both ^{2}H NMR [45, 31, 46, 12] and ^{1}H-^{13}C NMR techniques [40, 41, 42], see also Fig. 1. We call this phenomena *forking*, as done also previously to avoid confusion with splittings measured with NMR [43].

The forking has been studied in detail with ^{2}H NMR techniques by separately deuterating the R or S positions in CH_2 segments in order to assign order parameter to the correct hydrogen [12, 46]. These studies also show that the forking arises from differently sampled orientations of the two C–H bonds, not from two separate populations of lipid conformations [46, 12]. This means that realistic atomistic resolution molecular model has to reproduce the forking correctly and that the isomeric positions of the hydrogen must be taken into account when calculating order parameters from simulations [43].

2.8. Order parameters from simulations

Since all the atom coordinates are available from a molecular dynamics simulation trajectory, the order parameters can be calculated directly from the definition in Eq. 1. The ensemble average is taken over the simulation time and all the molecules in simulation. The hydrogen positions can be generated post-simulationally based on heavy atoms positions and the known hydrocarbon geometries for united atom simulations without explicit hydrogens by creating a trajectory with added hydrogens [88, 43] or by using equations to directly calculate order parameters [89, 90]. The first approach is appropriate for accurate structural studies since it allows to analyse forking in contrast to the latter technique.

The difference in the analysis methods for the forked segments is most likely the reason for diverging choline and glycerol backbone order parameters reported for the same models by different authors [91, 43]. Also different order parameters for C–H segments attached to double bond are reported for the same model [92, 88] due to a bug in a widely-used version of the *g_order* program in the Gromacs package. The *g_order* program also prints -S_{CH}, which is the most likely reason for the reported positive order parameters for acyl chains in some studies [93]. When these technical issues are taken into account, the different order parameters calculations from simulations are in good agreement.

The statistical error for order parameters is estimated by using the error of the mean for time blocks [88], independent simulations [91] and different lipids [43]. All these approaches yield a maximum error of $\sim \pm 0.01$.

It was recently pointed out that the sampling of individual dihedral angles might be very slow compared to the typical (100 ns) simulation timescales [94]. This result raises a question if the molecules sample the full phase phase during typical simulation time scales. On the other hand, another recent study showed that the slowest rotational auto-correlation function observed (for g_1 segment) in the Berger model reached a plateau (S^2_{CH}) after $\sim$200 ns and its relaxation was significantly too slow compared to NMR relaxation experiments [38], see Fig 8. This indicates that the typical simulation times are long enough for full conformational phase space sampling for the models with realistic dynamics [38].

2.9. Comparison between order parameters from simulations and experiments

The acyl chain order parameters are compared between simulations and experiments since the early days of lipid bilayer simulations [17, 95, 96, 97, 98, 99, 100, 101, 102, 103, 50, 89, 104]. Good agreement has been generally found [50, 51, 52, 53, 54, 55, 56, 57, 58, 36, 59, 60, 61, 62]. except for the C_2 segment of the *sn-2* chain having low magnitude and significant forking in all PC lipids, in contrast to C_2 of the chain linked to *sn*-1 [28, 45, 40, 41, 42], for example see Fig. 1 C). This feature is, however, not analyzed or not reproduced for several lipid models [51, 105, 55, 54, 53, 58, 57, 36, 60, 59]. Some models report the small order parameter for C_2, but the forking is not correctly reproduced or analyzed [105, 56, 36, 61]. Among all studied force fields, the united atom CHARMM36 is closest to the experimental results [62].

Also acyl chain order parameter changes with varying conditions are compared between simulations and experiments by several authors. Experimentally observed order parameter increase with cholesterol concentration [106, 107, 69, 108, 90, 42] and dehydration [71, 85] is observed also in simulations [109, 86, 90, 110, 111, 42, 112, 113], as well as the temperature induced order parameter decrease [69, 114]. A more careful comparison reveals, however, that the temperature and dehydration effects are slightly underestimated in simulations compared to experiments [86, 114]. Also cholesterol effects to DMPC bilayer are underestimated in the CHARMM36 model [111], while Slipids [112] and Amber Lipid14 [113] models show satisfactory agreement. The comparison of a Berger/Höltje [50, 115] based model to the extensive data set with various POPC/cholesterol mixtures shows good agreement with experiments for low cholesterol concentrations, however, the agreement gets worse for cholesterol concentration $\geq$ 34% [42]. A recent comparison of the Amber Lipid14 model to the same experimental data shows significantly better agreement, although slight overestimation of the ordering effect is observed with cholesterol concentration $\geq$ 34% [113], as shown in Fig. 5. The orientation of cholesterol ring structure in saturated or monounsaturated bilayers is reasonable in all models [90, 111, 42, 113], however, the cholesterol acyl chain exhibits too low order parameters in the Berger/Höltje [50, 115] based model [42] and too much forking in Amber Lipid14 [113], while CHARMM36 reproduces experiments well [111].

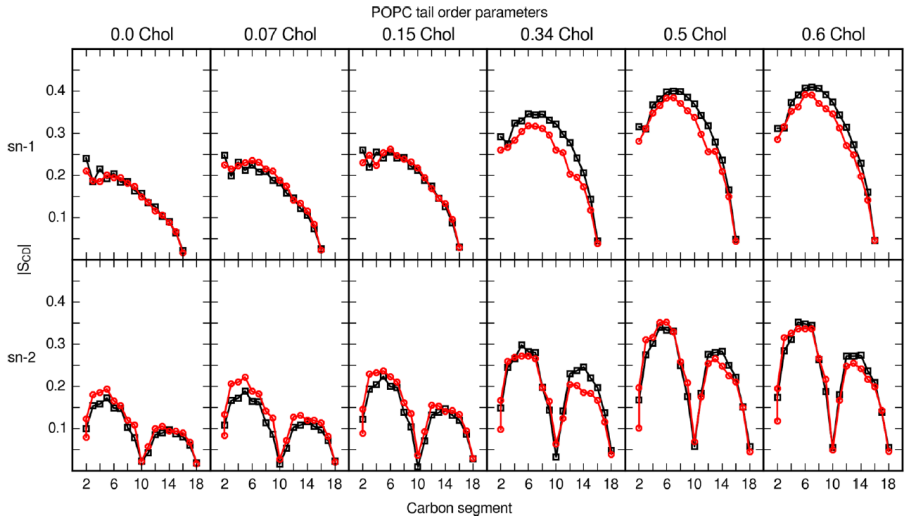

Figure 5: Cholesterol effect on acyl chain order parameters compared between the Amber Lipid14 model (black squares) [113] and experiments (red circles) [42] showing significantly better agreement than Berger/Höltje based model compared by Ferreira et al. [42] to the same experimental data. Reprinted with permission from Madej et al. J. Phys. Chem. B **2015**, 119, 12424-12435. Copyright 2015 American Chemical Society.

The dip of the acyl chain order parameter profile due to double bonds is generally reproduced by different simulation models [116, 117, 118, 119, 120, 121, 92, 122, 123, 88, 57, 56, 124, 42, 112, 62, 61]. The particularly good agreement, often achieved for the oleyl chain in POPC bilayer with one *cis* double bond, is demonstrated in Fig. 1 C). Also the further order parameter decrease due to multiple double bonds (polyunsaturation) [116, 117, 119, 120, 121, 92, 123, 88, 124] is usually well reproduced, as demonstrated in Fig. 6 for Berger [50] based model with double bond description by Bachar et al. [92]. Also difference between *cis* and *trans* double bonds can be reproduced in MD simulations [125].

In contrast to acyl chains, the glycerol backbone and choline order parameters are not routinely compared between simulations and experiments. In most comparisons the experimentally available signs, stereospecific labeling and high accuracy are not fully exploited [103, 86, 56, 91, 57, 43, 51, 20]. These issues were recently discussed by Botan et al. who also compared order parameters between 13 different simulation

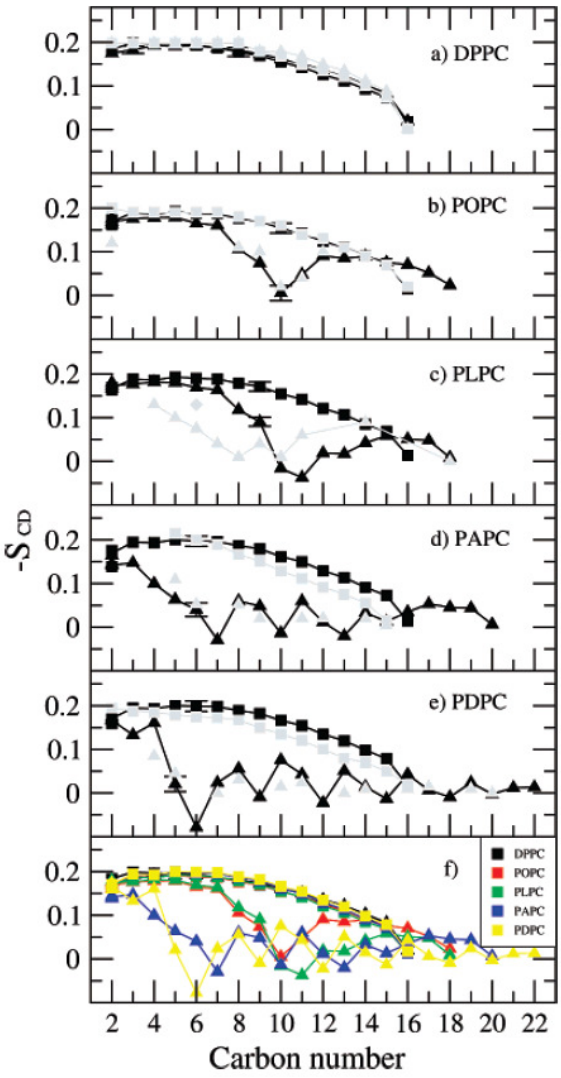

Figure 6: Figure comparing order parameters in polyunsaturated acyl chains between simulations and experiments [88]. Order parameters for the sn-1 (squares) and sn-2 (triangles) chains of (A) DPPC, (B) POPC, (C) PLPC, (D) PAPC, and (E) PDPC. Simulation results are shown in full black, and experimental results for comparison in gray. Additionally, part F summarizes the data for all bilayers from the simulations. Experimental order parameters were chosen for comparison as follows. The order parameters for DPPC (T=323K) are based on studies by Petrache et al. [126] whereas the experimental S_{CD} values for PDPC and for the sn-1 chain of POPC (T=310 K) are based on studies by Huber et al. [120] For the sn-1 chain of PDPC, the data set at 310 K is obtained by linearly interpolating between data at 303 and 323 K, whereas for the sn-2 chain the data at 303 K are presented [120]. Experimental values for the sn-2 chain of POPC are based on studies by Seelig et al. [31] A single experimental value is available also for the sn-2 chain of the PLPC bilayer at 313 K (diamond) [33] to compare with our simulated order parameters for PLPC. Together with PLPC, there are also experimental results for PiLPC (T=313K) [33]. Experimental order parameters for the sn-1 and sn-2 chains of PAPC (T=303 K) are based on quadrupole splittings measured by Rajamoorthi et al. [127]. For the sn-1 chain the monotonic decrease through the acyl chain is expected. For the sn-2 chain, values are fitted such that the agreement is as good as possible. Reprinted with permission from Ollila et al. J. Phys. Chem. B, **2007**, 111, 3139-3150. Copyright 2007 American Chemical Society.

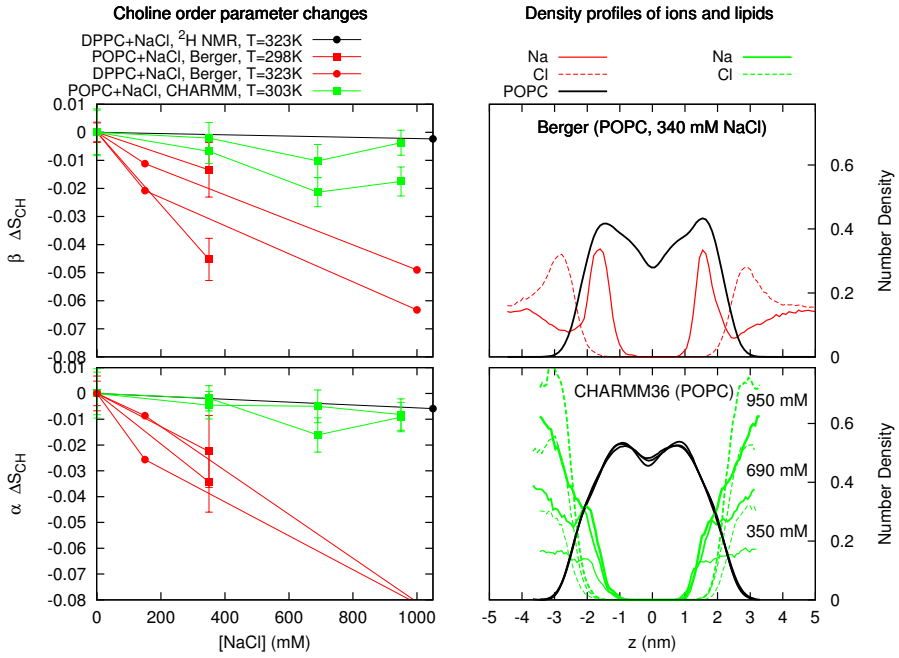

Figure 7: Changes in choline order parameters (left column) and ion density distributions (right column) as a function of NaCl concentration. Significant order parameter reduction and Na^+ partition is observed with Berger model while only modest order parameter change and ion partition observed with CHARMM36. The results are in line with the electrometer concept connecting the ion partition and choline order parameters changes [48, 72, 73, 74]. Consequently, the results show that Na^+ partition is significantly overestimated in the Berger model. For more discussion see [78].

models and experiments [43]. The results, shown also in Fig. 1 A), reveal significant differences between models and experiments, and none of the available models reproduces all order parameters within experimental error. On the other hand, experimentally observed choline order parameter increase with dehydration [49, 70, 85] and decrease due to cation binding [48, 72] were reproduced in simulations [43, 78]. However, especially the effect induced by Na^+ ion binding is strongly overestimated in several models which arises most likely from an artificially high partition coefficient [78], as also demonstrated in Fig. 7. The effect of cholesterol on glycerol backbone and choline is overestimated by the Berger/Höltje based [42] and Amber Lipid14 [113] models while CHARMM36 and MacRog performed better [43].

In conclusion, the acyl chain order parameters and their qualitative changes are

generally well described in atomistic MD models, except for C_2 segment in *sn*-2. However, all models have difficulties with varying severity to correctly describe the glycerol backbone and choline order parameters.

2.10. Interplay between simulations and NMR order parameters: Validation and interpretation

Since the acyl chain order parameters from MD models generally agree with experiments for single component lipid bilayers in full hydration, the conformations sampled in simulations can be considered as realistic atomistic resolution structures for the acyl chains (except for the C_2 segment in the *sn*-2 chain). As also the acyl chain rotational dynamics has the correct order of magnitude (see Section 3), the dynamical nature of hydrophobic region of lipid bilayers seen in simulation videos can be considered as a realistic representation of the system. This is significant advancement to the traditional static structural models [28, 128, 31, 33]. Since lipid bilayers are considered as a simple models for cell- and other biological membranes, the intuitive understanding of their dynamical nature has a significant impact on biomembrane physics and chemistry.

Also more detailed structural interpretation has been successful for acyl chain region, especially for order parameter decrease due to *cis* double bonds [121, 120, 129, 130, 131, 92, 88]. From NMR experiments alone it was not possible to judge if the order parameter decrease arises from the reduced chain order or the changes in average θ angle in Eq. 1 [130, 131]. The interpretation of NMR experiments with the help of MD simulations revealed that double bonds, indeed, decrease the chain order due to the flexible dihedral potentials next to the rigid double bonds [121, 120, 129, 130, 131, 92, 88].

The acyl chain order parameter increase and related bilayer thickening with cholesterol concentration [90, 110, 111, 42, 112, 113], dehydration [86, 109] and reduced temperature [114] are qualitatively reproduced by simulations giving intuitive visualizations for these effects. However, the order parameter changes are often under- or overestimated [86, 111, 114, 42], thus it is not clear how well the models can be used for atomistic resolution interpretation of these changes. For example, delicate lipid-cholesterol interactions are known to induce liquid-ordered and liquid-disordered phase coexistence [132]. To give atomistic resolution interpretation for this phenom-

ena [133, 134, 135, 136], the atomistic resolution structures and interactions should be correct, which does not seem to the case for several models [111, 42, 113].

Simulation studies have also predicted changes in the acyl chain region which are yet to be experimentally confirmed, e.g. order parameter decrease due to lipid oxidation and changes in order parameter sign in oxidized acyl chain [93].

The usability of MD models for structural interpretation decrease closer to the interfacial region since the experimental glycerol backbone, choline headgroup and *sn*-2 C_2 segment order parameters are not usually reproduced within experimental error, as discussed in the previous section. The forking and low order parameter values for C_2 in the *sn*-2 are related to the parallel orientation of the chain respect to membrane normal [128, 45] which is suggested to have significant contribution e.g. to membrane electrostatic potential [137] and acyl chain extended conformations [10]. Also the atomistic resolution structures sampled by glycerol backbone and choline headgroup are not yet fully resolved [29, 30, 32, 138, 35, 139]. Unfortunately, the accuracy of atomistic resolution models is not yet sufficient to solve these issues. However, the modeling of interfacial region structure has been getting more attention lately [56, 37, 57, 36, 43], thus higher quality models may be expected.

On the other hand, the increase of choline α and β order parameters with dehydration and decrease with cation binding were correctly reproduced by several models, despite of inaccurate choline structures [43, 78]. The order parameter increase was related to the choline P–N vector tilting more parallel to the membrane normal [43] and order parameter decrease to the cation binding affinity [78]. The observations are in line with previous studies on charge penetration [48, 72, 73, 74]. However, choline structural changes due to cholesterol or ion concentration are significantly overestimated in several models [42, 43, 78, 113], especially Na^+ binding affinity [78] (see also Fig. 7). The artificial specific Na^+ binding induces effectively positively charged membrane which may easily lead to erroneous conclusion due to dominant contribution of electrostatics for various phenomena.

In conclusion, the atomistic resolution MD simulations are invaluable in understanding the structural details and their changes in acyl chain region. However, in applications where lipid interfacial region structure, energetics, electrostatics or ion

distributions have significant role, the potential artifacts arising from simulation models must be carefully taken into account. A typical example of such application would be a study of interactions between charge containing protein in solution and lipid bilayer, simulated in physiological salt concentration [140, 141].

3. C-H bond rotational dynamics from spin relaxation rates and simulations

3.1. Definition and properties of rotational auto–correlation function

The second order auto-correlation function for the reorientation of the C–H chemical bond axis is defined as

$$g(\tau) = \langle P_2[\vec{\mu}(t) \cdot \vec{\mu}(t+\tau)] \rangle, \tag{4}$$

where P_2 denotes the second Legendre polynomial, $P_2(\xi) = 1/2(3\xi^2 - 1)$, $\vec{\mu}(t)$ is the unitary vector having the direction of the C–H bond at time t, and the angular brackets denote a time-average. For randomly oriented lamellar structures this auto–correlation is connected to the experimentally measurable spin relaxation rates through its Fourier transformation called spectral density [142].

$$j(\omega) = 2 \int_0^\infty \cos(\omega\tau) g(\tau) d\tau. \tag{5}$$

The auto–correlation function for bond orientations always decays to zero with long enough time scales in randomly oriented multilamellar samples due to the diffusion between differently oriented bilayer regions. However, the relaxation processes occur in two distinct timescales and the auto–correlation function can be written as a product of two independent functions [143, 38]

$$g(\tau) = g_{\mathrm{f}}(\tau) g_{\mathrm{s}}(\tau), \tag{6}$$

where $g_{\mathrm{f}}(\tau)$ describes the fast decay (faster than $\sim \mu$s) due to the lipid rotation within bilayer plane and $g_{\mathrm{s}}(\tau)$ describes the slow motions (slower than $\sim \mu$s) from the diffusion between differently oriented bilayer regions. The correlation time of 4.2 ms for

the slow decay was estimated from the spin-lattice relaxation rates in rotating frame $R_{1\rho}$, measured with different nutation frequencies for multilamellar POPC sample at 300K [38]. The full auto–correlation decaying to zero, including the contribution from the magic angle spinning (MAS) in kHz region [144], is illustrated in Fig. 8.

The $g_{\mathrm{f}}(\tau)$ decays to the plateau having value of S^2_{CH} within few hundred nanoseconds in liquid crystalline lipid bilayers with planar symmetry [38], as illustrated in Fig 8. The order parameters from ^{2}H NMR and ^{13}C NMR experiments are measured from this plateau [38], thus the rotational correlation function describes the average time needed to sample all conformations for a single molecule within the bilayer plane. The effective correlation time [145]

$$\tau_e := \int_0^\infty \frac{g_{\mathrm{f}}(\tau) - S^2_{\mathrm{CH}}}{1 - S^2_{\mathrm{CH}}} \mathrm{d}\tau \tag{7}$$

gives intuitive measure for this time; larger τ_e means longer time required for the conformational sampling. With this definition the area between the correlation function and its plateau becomes $(1 - S^2_{\mathrm{CH}})\tau_e$, as illustrated in Fig. 8.

3.2. Detecting C–H bond dynamics experimentally

The C–H bond dynamics in nanosecond timescales can be detected experimentally by measuring the spin relaxation rates R_1^C from ^{13}C NMR and R_1^D from ^{2}H NMR. These are connected the molecular dynamics through the spectral density (Eq. 5) and equations [142]

$$R_1^C = \frac{D^2_{\mathrm{max}} N_{\mathrm{H}}}{20} \Big[j(\omega_{\mathrm{H}} - \omega_{\mathrm{C}}) + 3j(\omega_{\mathrm{C}}) + 6j(\omega_{\mathrm{C}} + \omega_{\mathrm{H}}) \Big] \tag{8}$$

and

$$R_1^D = \frac{12\pi^2}{40} \left(\frac{e^2 q Q}{h} \right)^2 \Big[j(\omega_{\mathrm{D}}) + 4j(2\omega_{\mathrm{D}}) \Big], \tag{9}$$

where ω_{C}, ω_{H} and ω_{D} are the Larmor frequencies for ^{13}C, ^{1}H and ^{2}H, respectively, N_{H} is the number of bound protons, $\frac{D_{\mathrm{max}}}{2\pi}$ $\approx$22 kHz as in section 2.3 and $\frac{e^2 q Q}{h}$=170kHz as in section 2.2.

As seen from Eqs. 8 and 9, the numerical values of R_1^C and R_1^D depend on spectral

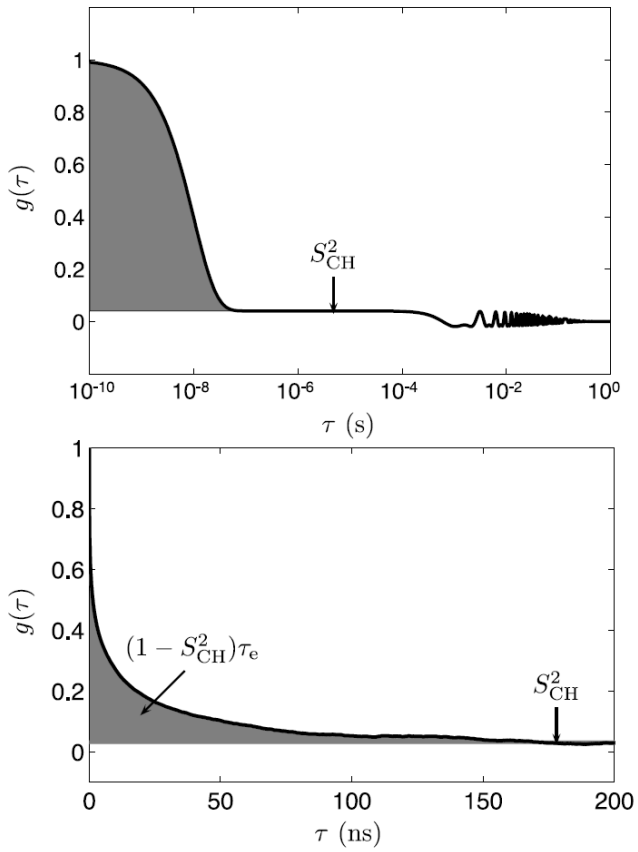

Figure 8: (Top) Illustration of the auto-correlation function $g(\tau)$ and effective correlation time τ_e for a ^{13}C-H bond in a lipid bilayer in MAS experiment (x–axis with logarithmic scale). Plateau after fast relaxation processes $g(\tau)_f$ is shown between roughly 10^{-7}s and 10^{-4}s. After this timescale the slow relaxation processes $g(\tau)_s$ and oscillation due to MAS [144] are shown. (Bottom) $g(\tau)$ for g_1 segment having the slowest relaxation in POPC bilayer simulated with the Berger based model, illustrating the decay towards S^2_{CH} (x–axis with linear scale). This represents the $g(\tau)_f$ in Eq. 6 and decrease to the plateau in the top figure. The effective correlation time τ_e is equal to the area in gray scaled by $(1 - S^2_{\mathrm{CH}})^{-1}$. Reprinted with permission from Ref. [38]. Copyright 2015 AIP Publishing LLC.

density values at the Larmor frequencies ω_C, ω_H and ω_D. On the other hand, the spectral density value for a given frequency ω depends on the relative amount of relaxation processes with timescales close to ω^{-1}. The Larmor frequencies depend on the spectrometer magnetic field strength and typical timescales for ω^{-1} are $\sim$1-20ns in ^{13}C NMR and ^{2}H NMR experiments. Thus, the R_1^C and R_1^D values measured with standard spectrometer with fixed external field strength gives a measure of relative amount of relaxation processes with the timescales $\sim$1-20ns. Further, the measured changes gives only the change of the relative amount of dynamical processes with the timescale detected, not the changes in sampling rate. For further discussion and demonstrations see e.g. [38].

For more comprehensive dynamical picture the spin relaxation parameters are measured with different magnetic field strengths by using the field cycling NMR [146, 147, 148, 84] or several spectrometers with different magnetic field strengths, as recently reviewed by Leftin and brown [65]. Also the model free approach to measure the effective correlation time (Eq. 7) was recently introduced [38]. The method is based on the combination of experimental order parameter S_{CH}, spin-lattice relaxation rates R_1^C and the transverse magnetization under a spin lock pulse $R_{1\rho}^{\mathrm{plateau}}$ measured with appropriate nutation frequency, given through equation

$$\tau_{\mathrm{e}} \approx \frac{5R_{1\rho}^{\mathrm{plateau}} - 3.82R_1^C}{D_{\mathrm{max}}^2 N_{\mathrm{H}}(1 - S_{\mathrm{CH}}^2)}. \tag{10}$$

3.3. Analyzing C–H bond dynamics from simulations

Since all the atom coordinates as a function of time are available from molecular dynamics simulations trajectory, the auto–correlation function for each C–H bond can be calculated directly from the definition in Eq. 4. The hydrogen positions can be generated post-simulationally based on heavy atoms positions and the known hydrocarbon geometries for united atom simulations without explicit hydrogens by creating a trajectory with added hydrogens [149, 150, 88, 38]. The ensemble average is taken over all the time intervals and molecules in present in simulation. Since the amount of data decreases for time intervals approaching the simulation total length, only interval lengths less than half of the total simulation time are typically used; for more details see [151].

To calculate the experimentally measurable spin lattice relaxation times from Eqs. 8 and 9, the spectral density must be first calculated from auto-correlation function using Eq. 5. Usually sum of 4 or more exponential are fitted to the calculated auto–correlation function and then analytical Fourier transform is used to calculate the spectral density [18, 152, 153, 129, 88, 38], however some authors have also used stretched exponential functions [149, 150]. The chosen functional form should not affect the spin relaxation rate values as long as the fit is good, however the correct form to describe the real relaxation process can be debated [65, 150, 154, 155, 156]. Single exponential function is not enough to describe relaxation observed in simulations while 4 gives a reasonable fit [129] which is not surprising since more than one relaxation timescales are expected to be present in bilayer lipids [18, 152, 153, 65]. The R_1^C and R_1^D values are straightforward to calculate from Eqs. 8 and 9 with different Larmor frequencies or as a function of external field by using the analytical spectral density function with fitted parameters.

The effective correlation time τ_e can be calculated directly from the integrated area below the correlation function, see Fig. 8 or by using the exponential sum fitted to the correlation function as in Eq. 30 of Ref. [38]. The $R_{1\rho}$, used to determine effective correlation time experimentally in Eq. 7 cannot be calculated from simulations directly since its value may depend also on the slow relaxation dynamics ($g_s(t)$ in Eq. 6) which is not present in simulations [38]. The same applies to the calculation of NOESY relaxations rates for which the decay time of 170 ns was assumed for the $g_s(t)$ [157], while 4.2 ms was measured by Ferreira et al. [38].

3.4. Comparing C–H bond dynamics between simulations and NMR experiments

Spin relaxation rates R_1^C and R_1^D with one [121, 129, 88, 104, 38] or more [18, 149, 153, 155, 104, 150, 124] external magnetic field strengths have been compared between experiments and simulations mainly for CHARMM (Fig. 9) and Berger based models (Fig. 10). The comparison with several magnetic field strengths shows good a agreement with large larmor frequencies for both CHARMM and Berger based models in Figs. 9 and 10 A), respectively. With increasing larmor frequencies both models show a good agreement deep in the acyl chain region while closer to the interfacial re-

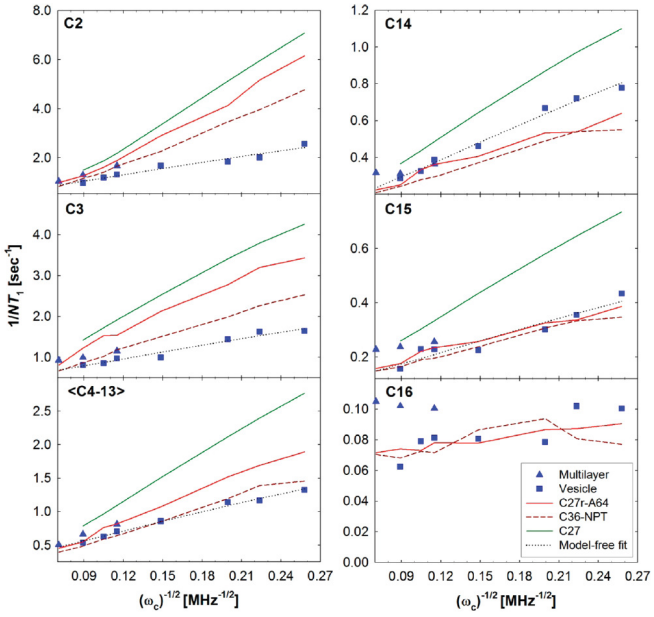

Figure 9: Comparison of R_1^C dependence on magnetic field between experiments [158, 155] and different CHARMM simulations [56] for acyl chain carbons (DPPC bilayer in 323K). Experiments as points; MD simulations as solid and dashed lines; and a model-free fit to the vesicle data as dotted lines. Reprinted with permission from Klauda et al. J. Phys. Chem. B, **2010**, 114, 7830-7843. Copyright 2010 American Chemical Society.

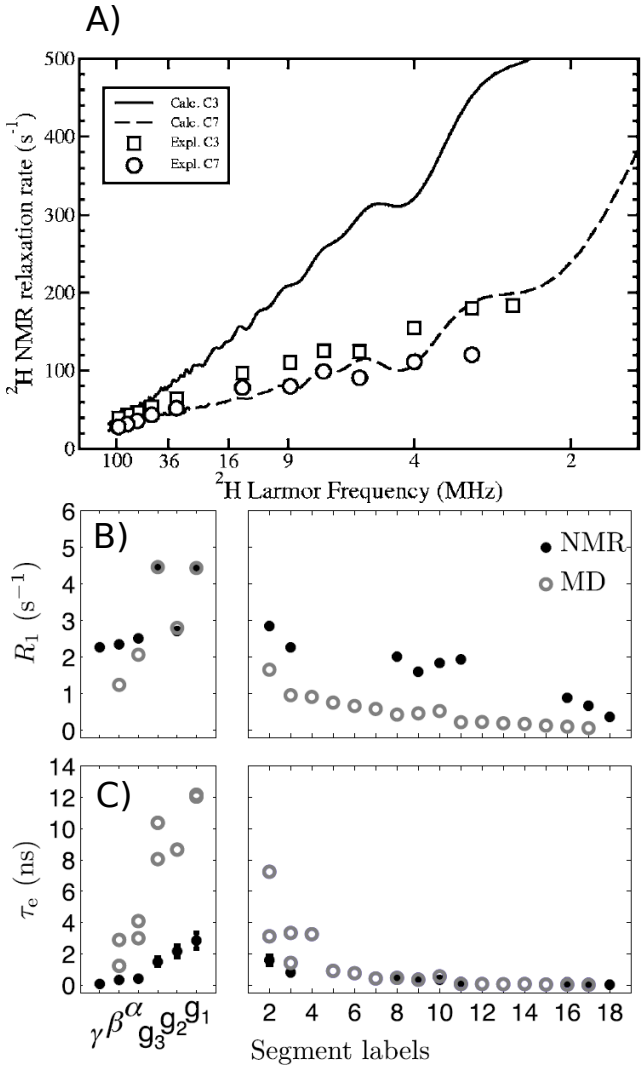

Figure 10: Comparisons between Berger based models and experimental spin relaxation rates: A) R_1^D dependence on magnetic field for acyl chain carbons (DMPC bilayer at 300K) [150]. Reprinted with permission from Ref. [150]. Copyright 2006 AIP Publishing LLC. B) R_1^C measured with field strength corresponding to the Larmor frequency of 125 MHz for ^{13}C (POPC bilayer at 298K) and C) effective correlation times τ_e (POPC bilayer at 298K). Reprinted with permission from Ref. [38]. Copyright 2015 AIP Publishing LLC.

gion motional modes corresponding lower Larmor frequencies seems to over-presented in both models. Since lower Larmor frequencies correspond longer correlation times, this may indicate too slow dynamics close to the interfacial region.

This is in line with the comparison between experimental and simulated effective correlation times for Berger based POPC model, shown in Fig. 10 C); the effective correlation times for acyl chain region agrees with experiments while closer to the interfacial region the correlation times are too large in simulations. The discrepancies for R_1^C between experiments and simulations for acyl chain region shown in Fig. 10 B) indicate, however, that different dynamical processes are not correctly balanced in simulations despite of good agreement for τ_e. On the other hand, spin relaxation rates for polyunsaturated acyl chains with large Larmor frequencies give reasonable values for both, CHARMM [129, 124] and Berger based [88] models.

3.5. Interplay between simulations and NMR spin lattice relaxation times: Validation and interpretation of dynamics

Most importantly, the fairly good agreement for spin relaxation rates and effective correlation times between simulations and experiments in acyl chain region indicates that the lipid rotational dynamics has the correct order of magnitude in simulations. Consequently, the rapid acyl chain fluctuations observed in simulations can be considered as realistic which further supports the advantage of simulation videos as an intuitive lipid bilayer picture compared to the traditional static pictures. While the molecular sampling rates seems to be underestimated closer to the interface, also the sampled structures are not exactly correct in simulations [43], thus the sampling rates in simulations are mainly interesting for people improving the models.

As discussed in Section 3.2 and for example in Ref. [38], single measured spin relaxation rate values or changes are not straightforwardly connected to the molecular dynamics. MD simulations can significantly ease this connection if the experimental spin relaxation rates or their differences can be reproduced [121, 129, 23]. This has been especially useful in the studies of polyunsaturated acyl chain dynamics which concluded – by combining the simulation and NMR relaxation data – that the double bonds speed up the chain dynamics due to flexible dihedrals next to the double

bonds [121, 129, 131, 130].

The successful interpretation of relaxation time measurements with MD is significantly less laborious than careful studies with different temperatures and magnetic field strengths, recently reviewed by Leftin and Brown [65]. On the other hand, the interpretation is also eased by the recently introduced effective correlation time experiments [38]. For example, careful compilation of several experimental data sets with different temperatures and magnetic fields was needed to conclude that the lipids has slower dynamics in interfacial region than in the acyl chains region [65], while the same conclusion is obvious from the measured effective correlation times in Fig. 10 [38]. The same is seen also in the MD simulations, however, the simulation model quality is not yet on the level to be used alone for interpretation for interfacial region.

Lipid bilayer rotational modes have been often interpreted with the wobble in the cone model [18, 153, 155, 156, 84] suggesting that the whole lipid molecule is wobbling as a cone and that all lipid segments share the same time scale for this motion. Further timescales for segmental dynamics then arises from the dynamics inside the cone. The auto–correlation functions predicted by the model are successfully fitted to the simulation and experimental data [18, 153, 155, 156, 84], however, fits with similar or better quality would be probably possible also with other type of models. In addition, significant changes of structure and dynamics experienced in the acyl chain region may not hinge on the headgroup [159, 43] indicating weak coupling between these segments, in line with one plausible interpretation for recent field cycling experiments [148]. Also the role of membrane undulations in the low frequency relaxation data is still under discussion [65, 154, 155, 156]. Thus, the wobbling in the cone is not yet fully proven to be the correct description for lipid rotational dynamics. Lipid models with realistic rotational dynamics for all segments with all timescales could elucidate this issue significantly.

4. Form factors from scattering and simulations

4.1. Form factor measured with X-ray or Neutron scattering

Small-angle X-ray or neutron scattering (SAXS/SANS) experiments can be used to probe the overall structure of the lipid bilayer, in particular scattering length density profiles along normal axis. The measured scattering intensity can be written as $I(q) \sim |F(q)|^2 S(q)/C_{\mathrm{LF}}$, where $F(q)$ is the bilayer form factor, $S(q)$ is the structure factor and C_{LF} the Lorentz correction ($C_{\mathrm{LF}} = q^2$ for free-floating lipid vesicles and $C_{\mathrm{LF}} = q$ for aligned bilayers). The structure factor characterizes the crystalline or quasi-crystalline structure of bilayer stacks and the form factor describes the scattering length density distribution of the lipid bilayer itself along the bilayer normal.

Here the main interest lies in the form factor since we focus on the lipid bilayer structure. The scattering intensity can be measured from unilamellar vesicles (ULVs) [16], oriented multilamellar bilayers (ORI) [160, 161] and un-oriented multilamellar vesicles (MLVs) [162]. Information about the structure factor is needed to extract the form factor from the scattering intensity, except for positionally uncorrelated ULVs, where $S(q) = 1$ [16]. For multibilayers in the fluid phase the structure factor is given by the Caillé theory [163, 160]. For oriented samples the form factor is determined by scaling a 2D fit of the Caillé structure factor (for in-plane and out-of-plane scattering contributions) to the measured scattering intensity [160, 161]. For MLVs the form factor needs to be modeled in combination with the structure factor to fit the scattering intensity [162]. This is achieved by using a specific real-space description of the bilayer structure (scattering length density profile). Note that different real-space model yield equivalent form factors. Thus, the form factors are not highly sensitive to the applied model. Different technical issues must be carefully considered in all scattering experiments, in particular subtracting background scattering and, in the case of ORI and MLVs, fitting accuracy. The form factors measured from different geometries [161, 164, 165] and research groups are in good agreement as demonstrated in Fig. 11, indicating that the bilayer structure is similar in different preparations of the same lipid and that the technique is highly robust.

By following the notation from Ref. [39], the form factor is connected to the bilayer

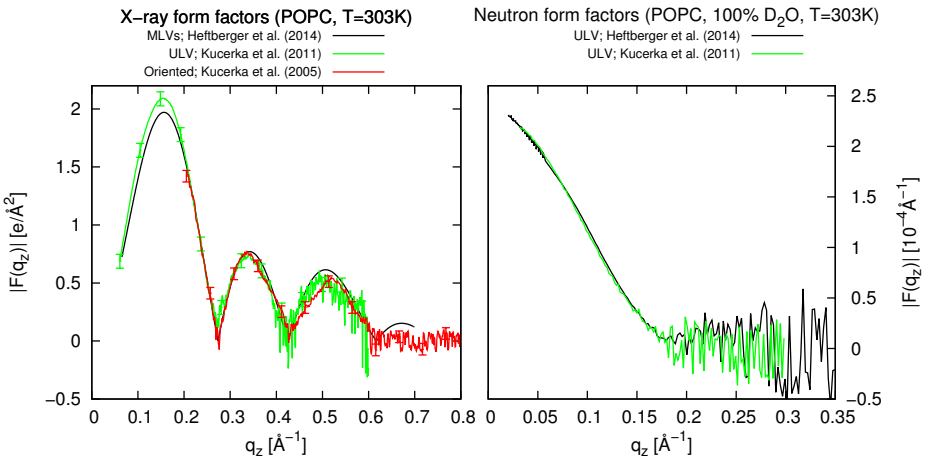

Figure 11: Comparison of reported X-ray (left panel) and neutron (right panel) form factors for POPC bilayers at 303K in different geometries measured by different groups: Heftberger et al. (2014) [162], Kucerka et al. (2011) [15] and Kucerka et al. (2005) [164]. The error bars given for neutron data by Kucerka et al. (2011) [15] are the same size as the line width.

atom number density through the equation

$$F(q) = \int_{-D/2}^{D/2} (\sum_{\alpha} f_{\alpha}(q_z) n_{\alpha}(z) - \rho_s) \exp(izq_z) \mathrm{d}z, \tag{11}$$

where $n_{\alpha}(z)$ is the atom α number density as a function of membrane normal coordinate z, $f_{\alpha}(q_z)$ is the atom scattering length density, ρ_s is the solvent scattering length density and integral spans over the bilayer of thickness D. The atom scattering length density $f_{\alpha}(q_z)$ depends on the type of scattering used since X-ray photons interact with the sample's electron cloud, while neutron scatter off nuclei in a particular manner. This leads also to distinct contrast for different parts of the membrane. X-rays, for example are most sensitive to the electron-rich phospholipid headgroups. Neutron experiments typically explore the contrast between hydrogen and deuterium [16], e.g. SANS on protiated lipid bilayers suspended in 100% D_2O probes mainly the membrane's hydrophobic thickness and specifically deuterated lipids are used to study lipid structural details [166, 167]. Also, e.g. ^{44}Ca has been used to detect Calcium location in lipid bilayer [168]. Consequently, highest-structural resolution can be achieved upon combining SAXS and SANS experiments [161, 169].

For symmetric lipid bilayers Eq. 11 simplifies to the widely used form

$$F(q) = \int_{-D/2}^{D/2} \Delta\rho_e(z) \cos(zq_z) \mathrm{d}z, \tag{12}$$

where $\Delta\rho_e(z)$ is the scattering length density difference between solvent and bilayer.

It should be noted that the form factor's sign cannot be determined directly from scattering experiments as all information on the phase is lost (known as the 'phase-problem' in diffraction), thus $|F(q)|$ is typically reported. However, the sign is practically determined by models for the bilayer structure used to extract the form factor from scattering intensity [39, 16] since only completely unphysical model would reproduce incorrent signs. Thus, the sign is not a useful quantity for assessing the high level accuracy of simulation data.

4.2. Form factor calculation from simulations

The atomic number densities $n_\alpha(z)$ are straightforward to calculate from simulations and then substitute into Eq. 11 to calculate the form factor. The atomic scattering length densities $f_\alpha(q_z)$ for neutrons are available in the literature [170]. For x-ray scattering point-wise valence electron location at the atom positions is usually assumed and in this case the $f_\alpha(q_z)$ becomes the number of electrons per atom, while also Gaussian electron distribution around atom positions [171] or an analytical expression $f_\alpha(q_z) = \sum_{j=1}^{4} a_j e^{-b_j (q/4\pi)^2} + c$ with parameters a_j, b_j and c taken from [172] are assumed in some studies [171], including the widely used SIMtoEXP software [39]. The effect of these choices to the electron density profiles was discussed by Benz et al. [171], however, it is not clear how strongly this would affect form factors calculated from simulations. In most simulations the bilayer is symmetric, thus the simpler Eq. 12 is used.

The small bilayer patches used in simulations might depress bilayer undulation modes which are present in large scale experiments [173]. Braun et al. showed that undulations seen in large simulations do not change the location of form factor minima but depress the peak heights in the lobes [173]. Since the undulations are expected to be present in the experiments, the potential discrepancies between simulations and

experiments in the lobe heights may be explained by the lack of undulation motions in simulations. The undulation effects are also sometimes reduced from the experimentally reported form factors by scaling q in x–axis, however, the scaling factor is very close to 1 [161].

Simulations give the form factors on absolute scale while experiments obtain them only on a relative scale, thus the experimental form factors from different sources has to be scaled for comparison [169, 39]. For example, the SIMtoEXP program uses the scaling factor k defined as

$$k = \frac{\sum_{i=1}^{N} \frac{|F_s(q_i)||F_e(q_i)|}{(\Delta F_e(q_i))^2}}{\sum_{i=1}^{N} \frac{|F_e(q_i)|^2}{(\Delta F_e(q_i))^2}}, \tag{13}$$

where $F_e(q)$ and $F_s(q)$ are experimental and simulated form factors, respectively, $\Delta F_e(q)$ is the uncertainty of the experimental form factor and the summation goes over all N data points [169, 39].

4.3. Comparing form factors between simulations and experiments

The comparison to experimental area per molecule values to validate the lipid density in simulations [89] has been nowadays often replaced with more direct comparison [6] using x-ray form factors [51, 55, 56, 57, 58, 111, 124, 112, 36, 62, 59, 61, 60, 113, 125]. In some studies the comparison is complemented with the comparison to the neutron scattering data with D_2O [57, 58, 62, 61, 60, 113]. In general the models produce form factors in good agreement with experiments for pure lipid bilayers, especially at small q values indicating that the overall bilayer dimensions, like thickness, are reproduced reasonably well. However, the agreement gets often worse toward higher q values [55, 56, 124, 57, 111, 58, 36, 112, 62, 59, 61, 125, 113] (see Fig. 12), indicating discrepancies in fine structural details such as, e.g. hydrocarbon chain packing or headgroup structure. Typically, the comparison of experimental and simulated form factors is based on visual inspection while also quantitative measure for simulated form factor quality has been suggested [39]. In some studies also Fourier transform coefficients are compared [171].

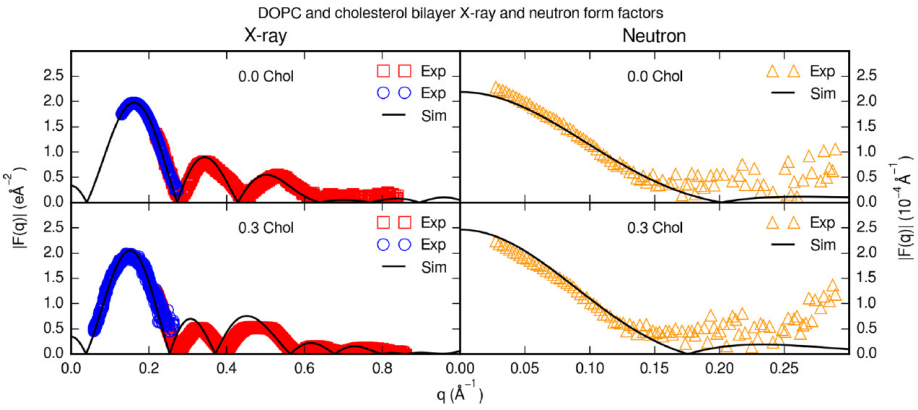

Figure 12: Comparison of experimental [174, 175] and simulated (using Amber Lipid14 [113]) X-ray and neutron form factors for pure DOPC bilayers and DOPC/cholesterol ($x_{chol} = 30$ mol%) mixtures. Within experimental uncertainty, simulations agree well with neutron data. For X-ray data, simulations match well DOPC experimental data at low q, but are slightly off for the third lobe, indicating some differences in the lipid bilayer fine structure. The DOPC/cholesterol mixture clearly shows disagreement between model and experiment for $q > 0.3\text{Å}^{-1}$. Overall, the simulated form factor minima are shifted toward lower q, revealing an overestimated bilayer thickening effect of cholesterol. Reprinted with permission from Madej et al. J. Phys. Chem. B **2015**, 119, 12424-12435. Copyright 2015 American Chemical Society.

Also changes in form factor due to temperature [58, 114], cholesterol concentration [112, 113] and acyl chain polyunsaturation [129, 124] have been compared between simulations and experiments [129, 161, 176, 177, 169, 174, 178, 15]. Simulation generally reproduce the decreased thickness and increased area with increasing temperature [58, 114] and polyunsaturation level [129, 124], as well as increased thickness and decreased area with increasing cholesterol concentration [112, 113]. However, the temperature dependence is underestimated for some systems [58, 114] while cholesterol effect is overestimated [112, 113], in good agreement with the comparisons to the NMR order parameter data [114, 113], as discussed in Section 2.9. Example of form factor comparison between experiments and simulations is shown in Fig. 12. Atomistic resolution simulations have not been able to reproduce the special cholesterol orientation, lying flat in the middle of polyunsaturated lipid bilayer, as observed with neutron scattering [179, 180, 181].

In conclusion, all the state of the art simulation models gives form factors close to experimental data in various conditions indicating reasonable agreement for average

bilayer dimensions. Also the qualitative changes are reproduced, however, discrepancies prevail for quantitative details of bilayer structure and changes with temperature and admixture of other lipids such as cholesterol.

4.4. Interplay between simulations and scattering experiments: Validation and interpretation

The scattering form factor gives accurate information about lipid bilayer structure but a model for atom number densities, $n_\alpha(z)$ in Eq. 11, is needed to resolve the structure, analogously to the NMR order parameters. Further, several atom density profiles can reproduce essentially the same form factor [169], thus also independent information is needed to confirm the structures suggested by the models, also analogously to the NMR order parameters. As already discussed in Section 2.1, significant advantage of MD model is that the same model can be straightforwardly compared to both, NMR and scattering data.

Several models, reviewed by Heberle et al. [182], are developed to give structural interpretation for the form factor data [183], while also MD simulations are used [184, 185, 169, 186, 187]. In these studies the area per molecule is often fixed to a value minimizing the differences between experimental and simulated form factors [184, 185, 169, 186, 187]. Depending on the model used, this area per molecule may be close to [187] or deviate significantly [184, 185, 169, 186] from the value predicted by the model in constant pressure simulations. However, with optimized area per molecule all models give form factors close to the experiments, despite of the bilayer tension generated in some models. On the other hand, comparisons between MD simulations and SDP model suggest small but measurable structural differences [169, 187]. The form factor from SDP model agrees better with experiments and structural parameters indicate differences especially in the glycerol backbone and the headgroup regions [169, 187], in agreement with comparison between simulations and NMR order parameters [43], as discussed in section 2.10.

More accurate understanding on the quality of interactions in lipid mixtures, e.g. with cholesterol is needed to use the simulations to interpret the scattering data from multicomponent systems [188] or the special cholesterol orientation in polyunsaturated

bilayers [179, 180, 181].

5. Conclusions

The comparisons of lipid bilayer C–H bond order parameters, spin relaxation rates and scattering form factors between MD simulations and experiments for the validation and interpretation of the sampled atomistic resolution structures are reviewed. The segmental order parameters and spin relaxation rates, measured with NMR, are related to the sampled structure and dynamics of individual molecules, while the scattering form factor is related to the average structure of the whole bilayer. NMR and scattering experiments are both highly robust and directly comparable to simulations, thus the sampled lipid and bilayer structures in MD model can be realistic only if these experimental quantities are reproduced with sufficient accuracy. Such an MD simulation model would be an ultimate tool to jointly interpret the NMR and scattering data. Further, such a model reproducing numerous independent experimental observables could be considered as the realistic atomistic resolution representation with high probability.

The current MD simulation models are yet not quite capable of achieving this goal. However, with current computational resources and available experimental data the community has a fair change to create truly realistic atomistic resolution representations of lipid bilayers. More specifically:

- Atomistic resolution MD simulations give realistic structures and rotational dynamics with correct order of magnitude for saturated and unsaturated acyl chains for PC lipid bilayers in full hydration close to 300K (or 323K for DPPC). Thus, the videos given by simulations can be considered as a realistic intuitive picture about the acyl chain region.
- Qualitative changes in the acyl chain region with temperature, dehydration and cholesterol are correctly described, however, in many cases the quality of detailed atomistic resolution changes are not clear.
- Current MD simulations are not yet accurate enough to resolve the atomistic resolution properties of glycerol backbone and choline regions, however, some structural changes can be correctly reproduced. Extreme care must be taken when simulation results are used to study, e.g. lipid–ion or lipid–cholesterol interactions on this region.

Similar conclusions are often made from the comparisons between simulations and two complementary experimental techniques, NMR and scattering, the first one related to the average properties of individual molecules and the latter to the average bilayer properties. In wider perspective it seems that atomistic MD simulations, NMR spectroscopy and scattering all gives complementary and coherent information on atomistic resolution biomolecular structure and dynamics. This indicates that the combination of these techniques has a realistic potential to generate atomistic resolution dynamical models of biomolecules in biologically relevant fluid state. However, the main barrier that currently needs to be overcome seems to be the quality of the interactions described in MD models.

The demand for atomistically accurate MD models will most likely increase in near future with increasing amount of accurate experimental data due the development in NMR methodology for lipids [42, 67, 68, 38, 189] and proteins [190], as well as due to the availability, e.g. wide-angle x-ray scattering of lipid bilayers, probing short-range positional correlations between hydrocarbons [191].

The inaccuracies of simulation models in the interfacial region may also hamper the simulation studies of different biochemical systems. For example, proteins approaching PC lipid bilayer in physiological NaCl concentration may encounter an effectively positively charged lipid bilayer due to artificial Na^+ binding with incorrect choline structure. In addition, the protein might sample incorrect states already in the bulk water [192, 193, 194]. From such a simulation it is difficult to filter results arising purely from simulation artifacts. Thus, improvements of force fields underlying MD simulations are strongly encouraged.

acknowledgements

This work is done by the NMRlipids Open Collaboration project running at `nmrlipids.blogspot.fi` and `https://github.com/NMRLipids`. We acknowledge Nobert kučerka and Frederick Heberle for sharing data for Fig. 11. Markus Miettinen and Peter Heftberger are acknowledged for useful comments. O.H.S.O. acknowledges financial

support by the Emil Aaltonen Foundation. G.P. acknowledges financial support by the Austrian Science Funds (FWF), grant no. P24459.

References

[1] J. Seelig, Deuterium magnetic resonance: theory and application to lipid membranes, Q. Rev. Biophys. 10 (1977) 353–418.

[2] J. N. Israelachvili, S. Marcelja, R. G. Horn, Physical principles of membrane organization, Q. Rev. Biophys. 13 (1980) 121–200.

[3] R. E. Jacobs, E. Oldfield, NMR of membranes, Prog. Nucl. Mag. Res. Sp. 14 (3) (1981) 113 – 136.

[4] J. H. Davis, The description of membrane lipid conformation, order and dynamics by ^{2}H-NMR, Biochim. Biophys. Acta 737 (1983) 117 – 171.

[5] M. Bloom, E. Evans, O. G. Mouritsen, Physical properties of the fluid lipid-bilayer component of cell membranes: a perspective, Q. Rev. Biophys. 24 (1991) 293–397.

[6] J. F. Nagle, S. Tristram-Nagle, Structure of lipid bilayers, Biochem. Biophys. Acta 1469 (2000) 159–195.

[7] J. F. Nagle, Introductory lecture: Basic quantities in model biomembranes, Faraday Discuss. 161 (2013) 11–29.

[8] A. G. Lee, How lipids affect the activities of integral membrane proteins, Biochim. Biophys. Acta 1666 (2004) 62–87.

[9] P. K. J. Kinnunen, Amyloid formation on lipid membrane surfaces, Open Biol. J. 2 (2009) 163–175.

[10] P. K. Kinnunen, K. Kaarniranta, A. K. Mahalka, Protein-oxidized phospholipid interactions in cellular signaling for cell death: From biophysics to clinical correlations, Biochim. Biophys. Acta 1818 (2012) 2446 – 2455.

[11] M. Bohdanowicz, S. Grinstein, Role of phospholipids in endocytosis, phagocytosis, and macropinocytosis, Physiol. Rev. 93 (1) (2013) 69–106.

[12] H. U. Gally, G. Pluschke, P. Overath, J. Seelig, Structure of escherichia coli membranes. glycerol auxotrophs as a tool for the analysis of the phospholipid head-group region by deuterium magnetic resonance, Biochemistry 20 (7) (1981) 1826–1831.

[13] P. Scherer, J. Seelig, Structure and dynamics of the phosphatidylcholine and the phosphatidylethanolamine head group in L-M fibroblasts as studied by deuterium nuclear magnetic resonance, EMBO J. 6.

[14] G. Pabst, N. Kučerka, M.-P. Nieh, M. Rheinstädter, J. Katsaras, Applications of neutron and x-ray scattering to the study of biologically relevant model membranes, Chem. Phys. Lipids 163 (2010) 460 – 479.

[15] N. Kučerka, M. P. Nieh, J. Katsaras, Fluid phase lipid areas and bilayer thicknesses of commonly used phosphatidylcholines as a function of temperature, Biochim. Biophys. Acta 1808 (11) (2011) 2761–2771.

[16] D. Marquardt, F. A. Heberle, J. D. Nickels, G. Pabst, J. Katsaras, On scattered waves and lipid domains: detecting membrane rafts with x-rays and neutrons, Soft Matter 11 (2015) 9055–9072.

[17] P. van der Ploeg, H. J. C. Berendsen, Molecular dynamics simulation of a bilayer membrane, J. Chem. Phys. 76 (6) (1982) 3271–3276.

[18] R. W. Pastor, R. M. Venable, M. Karplus, A. Szabo, A simulation based model of NMR T1 relaxation in lipid bilayer vesicles, J. Chem. Phys. 89 (2) (1988) 1128–1140.

[19] R. Wohlgemuth, N. Waespe-Sarcevic, J. Seelig, Bilayers of phosphatidylglycerol. A deuterium and phosphorus nuclear magnetic resonance study of the headgroup region, Biochemistry 19 (1980) 3315–3321.

[20] J. Kapla, B. Stevensson, M. Dahlberg, A. Maliniak, Molecular dynamics simulations of membranes composed of glycolipids and phospholipids, J. Phys. Chem. B 116 (2012) 244–252.

[21] J. Pan, X. Cheng, F. A. Heberle, B. Mostofian, N. Kučerka, P. Drazba, J. Katsaras, Interactions between ether phospholipids and cholesterol as determined by scattering and molecular dynamics simulations, J. Phys. Chem. B 116 (51) (2012) 14829–14838.

[22] N. Kučerka, B. W. Holland, C. G. Gray, B. Tomberli, J. Katsaras, Scattering density profile model of POPG bilayers as determined by molecular dynamics simulations and small-angle neutron and x-ray scattering experiments, J. Phys. Chem. B 116 (2012) 232–239.

[23] A. Nowacka, N. Bongartz, O. Ollila, T. Nylander, D. Topgaard, Signal intensities in ^{1}H–^{13}C CP and INEPT MAS NMR of liquid crystals, J. Magn. Res. 230 (2013) 165 – 175.

[24] J. Pan, X. Cheng, L. Monticelli, F. A. Heberle, N. Kucerka, D. P. Tieleman, J. Katsaras, The molecular structure of a phosphatidylserine bilayer determined by scattering and molecular dynamics simulations, Soft Matter 10 (2014) 3716–3725.

[25] A. L. Boscia, B. W. Treece, D. Mohammadyani, J. Klein-Seetharaman, A. R. Braun, T. A. Wassenaar, B. Klösgen, S. Tristram-Nagle, X-ray structure, thermodynamics, elastic properties and MD simulations of cardiolipin/dimyristoylphosphatidylcholine mixed membranes, Chem. Phys. Lipids 178 (2014) 1 – 10.

[26] T. M. Ferreira, D. Topgaard, O. H. S. Ollila, Molecular conformation and bilayer pores in a nonionic surfactant lamellar phase studied with ^{1}H–^{13}C solid–state NMR and molecular dynamics simulations, Langmuir 30 (2) (2014) 461–469.

[27] A. Abragam, The Principles of Nuclear Magnetism, Oxford University Press, 1961.

[28] A. Seelig, J. Seelig, Dynamic structure of fatty acyl chains in a phospholipid bilayer measured by deuterium magnetic resonance, Biochemistry 13 (23) (1974) 4839–4845.

[29] H. U. Gally, W. Niederberger, J. Seelig, Conformation and motion of the choline head group in bilayers of dipalmitoyl-3-sn-phosphatidylcholine, Biochemistry 14 (16) (1975) 3647–3652.

[30] A. Seelig, J. Seelig, Effect of a single *cis* double bond on the structure of a phospholipid bilayer, Biochemistry 16 (1977) 45–50.

[31] J. Seelig, N. Waespe-Sarcevic, Molecular order in *cis* and *trans* unsaturated phospholipid bilayers, Biochemistry 17 (1978) 3310–3315.

[32] L. Strenk, P. Westerman, J. Doane, A model of orientational ordering in phosphatidylcholine bilayers based on conformational analysis of the glycerol backbone region, Biophys. J. 48 (5) (1985) 765 – 773.

[33] J. E. Baenziger, H. C. Jarrel, R. J. Hill, I. C. P. Smith, Average structural and motional properties of diunsaturated acyl chain in a lipid bilayer: Effects of two *cis*-unsaturated double bonds, Biochemistry 30 (1991) 894–903.

[34] M. Hong, K. Schmidt-Rohr, D. Nanz, Study of phospholipid structure by ^{1}H, ^{13}C, and ^{31}P dipolar couplings from two-dimensional NMR, Biophys. J. 69 (1995) 1939 – 1950.

[35] K. S. Bruzik, J. S. Harwood, Conformational study of phospholipids in crystalline state and hydrated bilayers by ^{13}C and ^{31}P CP-MAS NMR, J. Am. Chem. Soc. 119 (1997) 6629–6637.

[36] J. Chowdhary, E. Harder, P. E. M. Lopes, L. Huang, A. D. MacKerell, B. Roux, A polarizable force field of dipalmitoylphosphatidylcholine based on the classical drude model for molecular dynamics simulations of lipids, J. Phys. Chem. B 117 (31) (2013) 9142–9160.

[37] P. Prakash, R. Sankararamakrishnan, Force field dependence of phospholipid headgroup and acyl chain properties: Comparative molecular dynamics simulations of dmpc bilayers, J. Comp. Chem. 31 (2) (2010) 266–277.

[38] T. M. Ferreira, O. H. S. Ollila, R. Pigliapochi, A. P. Dabkowska, D. Topgaard, Model-free estimation of the effective correlation time for CH bond reorientation in amphiphilic bilayers: ^{1}H-^{13}C solid-state NMR and MD simulations, J. Chem. Phys. 142 (2015) 044905.

[39] N. Kučerka, J. Katsaras, J. Nagle, Comparing membrane simulations to scattering experiments: Introducing the SIMtoEXP software, J. Membr. Biol. 235 (1) (2010) 43–50.

[40] J. D. Gross, D. E. Warschawski, R. G. Griffin, Dipolar recoupling in MAS NMR: a probe for segmental order in lipid bilayers, J. Am. Chem. Soc. 119 (4) (1997) 796–802.

[41] S. V. Dvinskikh, V. Castro, D. Sandström, Efficient solid-state NMR methods for measuring heteronuclear dipolar couplings in unoriented lipid membrane systems, Phys. Chem. Chem. Phys. 7 (2005) 607–613.

[42] T. M. Ferreira, F. Coreta-Gomes, O. H. S. Ollila, M. J. Moreno, W. L. C. Vaz, D. Topgaard, Cholesterol and POPC segmental order parameters in lipid membranes: solid state ^{1}H-^{13}C NMR and MD simulation studies, Phys. Chem. Chem. Phys. 15 (2013) 1976–1989.

[43] A. Botan, F. Favela-Rosales, P. F. J. Fuchs, M. Javanainen, M. Kanduč, W. Kulig, A. Lamberg, C. Loison, A. Lyubartsev, M. S. Miettinen, L. Monticelli, J. Määttä, O. H. S. Ollila, M. Retegan, T. Róg, H. Santuz, J. Tynkkynen, Toward atomistic resolution structure of phosphatidylcholine headgroup and glycerol backbone at different ambient conditions, J. Phys. Chem. B 119 (2015) 15075–15088.

[44] M. Hong, K. Schmidt-Rohr, A. Pines, NMR measurement of signs and magnitudes of C-H dipolar couplings in lecithin, J. Am. Chem. Soc. 117 (1995) 3310–3311.

[45] A. Seelig, J. Seelig, Bilayers of dipalmitoyl-3-sn-phosphatidylcholine: Conformational differences between the fatty acyl chains, Biochim. Biophys. Acta 406 (1975) 1 – 5.

[46] A. K. Engel, D. Cowburn, The origin of multiple quadrupole couplings in the deuterium NMR spectra of the 2 chain of 1,2 dipalmitoyl-sn-glycero-3-phosphorylcholine, FEBS Lett. 126 (1981) 169 – 171.

[47] B. Perly, I. C. P. Smith, H. C. Jarrell, Effects of the replacement of a double bond by a cyclopropane ring in phosphatidylethanolamines: a deuterium NMR study of phase transitions and molecular organization, Biochemistry 24 (4) (1985) 1055–1063.

[48] H. Akutsu, J. Seelig, Interaction of metal ions with phosphatidylcholine bilayer membranes, Biochemistry 20 (1981) 7366–7373.

[49] B. Bechinger, J. Seelig, Conformational changes of the phosphatidylcholine headgroup due to membrane dehydration. a ^{2}H-NMR study, Chem. Phys. Lipids 58 (1991) 1 – 5.

[50] O. Berger, O. Edholm, F. Jähnig, Molecular dynamics simulations of a fluid bilayer of dipalmitoylphosphatidylcholine at full hydration, constant pressure, and constant temperature, Biophys. J. 72 (1997) 2002 – 2013.

[51] C.-J. Högberg, A. M. Nikitin, A. P. Lyubartsev, Modification of the CHARMM force field for DMPC lipid bilayer, J. Comput. Chem. 29 (14) (2008) 2359–2369.

[52] D. Poger, W. F. Van Gunsteren, A. E. Mark, A new force field for simulating phosphatidylcholine bilayers, J. Comput. Chem. 31 (6) (2010) 1117–1125.

[53] J. P. Ulmschneider, M. B. Ulmschneider, United atom lipid parameters for combination with the optimized potentials for liquid simulations all-atom force field, J. Chem. Theory Comput. 5 (7) (2009) 1803–1813.

[54] A. Kukol, Lipid models for united-atom molecular dynamics simulations of proteins, J. Chem. Theory Comput. 5 (3) (2009) 615–626.

[55] S.-W. Chiu, S. A. Pandit, H. L. Scott, E. Jakobsson, An improved united atom force field for simulation of mixed lipid bilayers, J. Phys. Chem. B 113 (9) (2009) 2748–2763.

[56] J. B. Klauda, R. M. Venable, J. A. Freites, J. W. O'Connor, D. J. Tobias, C. Mondragon-Ramirez, I. Vorobyov, A. D. MacKerell Jr, R. W. Pastor, Update of the CHARMM all-atom additive force field for lipids: Validation on six lipid types, J. Phys. Chem. B 114 (2010) 7830–7843.

[57] C. J. Dickson, L. Rosso, R. M. Betz, R. C. Walker, I. R. Gould, GAFFlipid: a general amber force field for the accurate molecular dynamics simulation of phospholipid, Soft Matter 8 (2012) 9617–9627.

[58] J. P. M. Jämbeck, A. P. Lyubartsev, Derivation and systematic validation of a refined all-atom force field for phosphatidylcholine lipids, J. Phys. Chem. B 116 (10) (2012) 3164–3179.

[59] A. Maciejewski, M. Pasenkiewicz-Gierula, O. Cramariuc, I. Vattulainen, T. Róg, Refined OPLS all-atom force field for saturated phosphatidylcholine bilayers at full hydration, J. Phys. Chem. B 118 (17) (2014) 4571–4581.

[60] R. Tjörnhammar, O. Edholm, Reparameterized united atom model for molecular dynamics simulations of gel and fluid phosphatidylcholine bilayers, J. Chem. Theory Comput. 10 (12) (2014) 5706–5715.

[61] C. J. Dickson, B. D. Madej, A. A. Skjevik, R. M. Betz, K. Teigen, I. R. Gould, R. C. Walker, Lipid14: The amber lipid force field, J. Chem. Theory Comput. 10 (2) (2014) 865–879.

[62] S. Lee, A. Tran, M. Allsopp, J. B. Lim, J. Henin, J. B. Klauda, CHARMM36 united atom chain model for lipids and surfactants, J. Phys. Chem. B 118 (2) (2014) 547–556.

[63] V. Castro, S. V. Dvinskikh, G. Widmalm, D. Sandstrm, A. Maliniak, NMR studies of membranes composed of glycolipids and phospholipids, Biochim. Biophys. Acta 1768 (10) (2007) 2432 – 2437.

[64] V. Castro, B. Stevensson, S. V. Dvinskikh, C.-J. Högberg, A. P. Lyubartsev, H. Zimmermann, D. Sandström, A. Maliniak, NMR investigations of interactions between anesthetics and lipid bilayers, Biochim. Biophys. Acta 1778 (2008) 2604 – 2611.

[65] A. Leftin, M. F. Brown, An NMR database for simulations of membrane dynamics, Biochim. Biophys. Acta - Biomembranes 1808 (2011) 818 – 839.

[66] D. Marsh, Handbook of Lipid Bilayers, Second Edition, RSC press, 2013.

[67] A. Leftin, C. Job, K. Beyer, M. F. Brown, Solid-state ^{13}C NMR reveals annealing of raft-like membranes containing cholesterol by the intrinsically disordered protein -synuclein, Journal of Molecular Biology 425 (16) (2013) 2973 – 2987.

[68] A. Leftin, T. Molugu, C. Job, K. Beyer, M. Brown, Area per lipid and cholesterol interactions in membranes from separated local-field ^{13}C NMR spectroscopy, Biophys. J. 107 (10) (2014) 2274 – 2286.

[69] J. Douliez, A. Lonard, E. Dufourc, Restatement of order parameters in biomembranes: calculation of C-C bond order parameters from C-D quadrupolar splittings, Biophys. J. 68 (5) (1995) 1727 – 1739.

[70] A. Ulrich, A. Watts, Molecular response of the lipid headgroup to bilayer hydration monitored by ^{2}H-NMR, Biophys. J. 66 (1994) 1441 – 1449.

[71] K. Mallikarjunaiah, A. Leftin, J. J. Kinnun, M. J. Justice, A. L. Rogozea, H. I. Petrache, M. F. Brown, Solid-state ^{2}H NMR shows equivalence of dehydration and osmotic pressures in lipid membrane deformation, Biophys. J. 100 (1) (2011) 98 – 107.

[72] C. Altenbach, J. Seelig, Calcium binding to phosphatidylcholine bilayers as studied by deuterium magnetic resonance. Evidence for the formation of a calcium complex with two phospholipid molecules, Biochemistry 23 (1984) 3913–3920.

[73] J. Seelig, P. M. MacDonald, P. G. Scherer, Phospholipid head groups as sensors of electric charge in membranes, Biochemistry 26 (24) (1987) 7535–7541.

[74] P. G. Scherer, J. Seelig, Electric charge effects on phospholipid headgroups. phosphatidylcholine in mixtures with cationic and anionic amphiphiles, Biochemistry 28 (1989) 7720–7728.

[75] M. F. Brown, J. Seelig, Influence of cholesterol on the polar region of phosphatidylcholine and phosphatidylethanolamine bilayers, Biochemistry 17 (1978) 381–384.

[76] E. Kuchinka, J. Seelig, Interaction of melittin with phosphatidylcholine membranes. binding isotherm and lipid head-group conformation, Biochemistry 28 (10) (1989) 4216–4221.

[77] M. Roux, M. Bloom, Calcium, magnesium, lithium, sodium, and potassium distributions in the headgroup region of binary membranes of phosphatidylcholine and phosphatidylserine as seen by deuterium NMR, Biochemistry 29 (30) (1990) 7077–7089.

[78] A. Catte, M. Girych, M. Javanainen, M. S. Miettinen, L. Monticelli, J. Määttä, V. S. Oganesyan, O. H. S. Ollila, The electrometer concept and binding of cations to phospholipid bilayers, DOI: 10.5281/zenodo.32175 (2015).

[79] F. Aussenac, M. Laguerre, J.-M. Schmitter, E. J. Dufourc, Detailed structure and dynamics of bicelle phospholipids using selectively deuterated and perdeuterated labels. ^{2}H NMR and molecular mechanics study, Langmuir 19 (25) (2003) 10468–10479.

[80] G. Raffard, S. Steinbruckner, A. Arnold, J. H. Davis, E. J. Dufourc, Temperature–composition diagram of dimyristoylphosphatidylcholine-dicaproylphosphatidylcholine ”bicelles” self-orienting in the magnetic field. A solid state ^{2}H and ^{31}P NMR study, Langmuir 16 (20) (2000) 7655–7662.

[81] C. R. Sanders, J. P. Schwonek, Characterization of magnetically orientable bilayers in mixtures of dihexanoylphosphatidylcholine and dimyristoylphosphatidylcholine by solid-state NMR, Biochemistry 31 (37) (1992) 8898–8905.

[82] L. E. Marbella, B. Yin, M. M. Spence, Investigating the order parameters of saturated lipid molecules under various curvature conditions on spherical supported lipid bilayers, J. Phys. Chem. B 119 (11) (2015) 4194–4202.

[83] J. Becker, A. Comotti, R. Simonutti, P. Sozzani, K. Saalwchter, Molecular motion of isolated linear alkanes in nanochannels, J. Phys. Chem. B 109 (49) (2005) 23285–23294.

[84] V. N. Sivanandam, J. Cai, A. G. Redfield, M. F. Roberts, Phosphatidylcholine wobble in vesicles assessed by high-resolution ^{13}C field cycling NMR spectroscopy, J. Am. Chem. Soc. 131 (10) (2009) 3420–3421.

[85] S. V. Dvinskikh, V. Castro, D. Sandstrom, Probing segmental order in lipid bilayers at variable hydration levels by amplitude- and phase-modulated cross-polarization NMR, Phys. Chem. Chem. Phys. 7 (2005) 3255–3257.

[86] C.-J. Högberg, , A. P. Lyubartsev, A molecular dynamics investigation of the influence of hydration and temperature on structural and dynamical properties of a dimyristoylphosphatidylcholine bilayer, J. Phys. Chem. B 110 (29) (2006) 14326–14336.

[87] The nmrlipids project, on the signs of the order parameters (2014).
URL http://web.archive.org/web/20150414085027/http://nmrlipids.blogspot.fi/2014/04/on-signs-of-order-parameters.html

[88] S. Ollila, M. T. Hyvönen, I. Vattulainen, Polyunsaturation in lipid membranes: Dynamic properties and lateral pressure profiles, J. Phys. Chem. B 111 (2007) 3139–3150.

[89] D. P. Tieleman, S. J. Marrink, H. J. C. Berendsen, A computer perspective of membranes: molecular dynamics studies of lipid bilayer systems, Biochim. Biophys. Acta 1331 (1997) 235–270.

[90] L. Vermeer, B. de Groot, V. Rat, A. Milon, J. Czaplicki, Acyl chain order parameter profiles in phospholipid bilayers: computation from molecular dynamics simulations and comparison with ^{2}H NMR experiments, Eur. Biophys. J. 36 (8) (2007) 919–931.

[91] D. Poger, A. E. Mark, Lipid bilayers: The effect of force field on ordering and dynamics, J. Chem. Theory Comput. 8 (11) (2012) 4807–4817.

[92] M. Bachar, P. Brunelle, D. P. Tieleman, A. Rauk, Molecular dynamics simulation of a polyunsaturated lipid bilayer susceptible to lipid peroxidation, J. Phys. Chem. B 108 (2004) 7170–7179.

[93] J. Wong-ekkabut, Z. Xu, W. Triampo, I.-M. Tang, D. P. Tieleman, L. Monticelli, Effect of lipid peroxidation on the properties of lipid bilayers: A molecular dynamics study, Biophys. J. 93 (12) (2007) 4225 – 4236.

[94] A. Vogel, S. Feller, Headgroup conformations of phospholipids from molecular dynamics simulation: Sampling challenges and comparison to experiment, J. Membr. Biol. 245 (2012) 23–28.

[95] E. Egberts, H. J. C. Berendsen, Molecular dynamics simulation of a smectic liquid crystal with atomic detail, J. Chem. Phys. 89 (1988) 3718–3732.

[96] T. R. Stouch, Lipid membrane structure and dynamics studied by all-atom molecular dynamics simulations of hydrated phospholipid bilayers, Mol. Simul. 10 (1993) 335–362.

[97] E. Egberts, S.-J. Marrink, H. Berendsen, Molecular dynamics simulation of a phospholipid membrane, Eur. Biophys. J. 22 (6) (1994) 423–436.

[98] J. W. Essex, M. M. Hann, W. G. Richards, Molecular dynamics simulation of a hydrated phospholipid bilayer, Philos. T. Roy. Soc. B 344 (1309) (1994) 239–260.

[99] A. Robinson, W. Richards, P. Thomas, M. Hann, Head group and chain behavior in biological membranes: a molecular dynamics computer simulation, Biophys. J. 67 (6) (1994) 2345 – 2354.

[100] M. T. Hyvönen, M. Ala-Korpela, J. Vaara, T. T. Rantala, J. Jokisaari, Effects of two double bonds on the hydrocarbon interior of a phospholipid bilayer, Chem. Phys. Lett. 246 (1995) 300–306.

[101] V. Kothekar, Molecular dynamics simulation of hydrated phospholipid bilayers, Ind. J. Biochem. Biophys. 33 (1996) 431 – 447.

[102] D. P. Tieleman, H. J. C. Berendsen, Molecular dynamics simulations of a fully hydrated dipalmitoylphosphatidylcholine bilayer with different macroscopical boundary conditions and parameters, J. Chem. Phys. 105 (1996) 4871–4880.

[103] W. Shinoda, N. Namiki, S. Okazaki, Molecular dynamics study of a lipid bilayer: Convergence, structure, and long-time dynamics, J. Chem. Phys. 106 (13) (1997) 5731–5743.

[104] J. B. Klauda, R. M. Venable, A. D. M. Jr., R. W. Pastor, Considerations for lipid force field development, in: S. E. Feller (Ed.), Computational Modeling of Membrane Bilayers, Vol. 60 of Current Topics in Membranes, Academic Press, 2008, pp. 1 – 48.

[105] S. W. I. Siu, R. Vácha, P. Jungwirth, R. A. Böckmann, Biomolecular simulations of membranes: Physical properties from different force fields, J. Chem. Phys. 128 (2008) 125103.

[106] E. J. Dufourc, E. J. Parish, S. Chitrakorn, I. C. P. Smith, Structural and dynamical details of cholesterol-lipid interaction as revealed by deuterium NMR, Biochemistry 23 (25) (1984) 6062–6071.

[107] M. Lafleur, P. Cullis, M. Bloom, Modulation of the orientational order profile of the lipid acyl chain in the l phase, Eur. Biophys. J. 19 (2) (1990) 55–62.

[108] J. A. Urbina, S. Pekerar, H. biao Le, J. Patterson, B. Montez, E. Oldfield, Molecular order and dynamics of phosphatidylcholine bilayer membranes in the presence of cholesterol, ergosterol and lanosterol: a comparative study using ^{2}H-, ^{13}C- and ^{31}P-NMR spectroscopy, Biochim. Biophys. Acta 1238 (2) (1995) 163 – 176.

[109] R. J. Mashl, H. L. Scott, S. Subramaniam, E. Jakobsson, Molecular simulation of dioleoylphosphatidylcholine lipid bilayers at differing levels of hydration, Biophys. J. 81 (6) (2001) 3005 – 3015.

[110] Q. Zhu, K. H. Cheng, M. W. Vaughn, Molecular dynamics studies of the molecular structure and interactions of cholesterol superlattices and random domains in an unsaturated phosphatidylcholine bilayer membrane, J. Phys. Chem. B 111 (37) (2007) 11021–11031.

[111] J. B. Lim, B. Rogaski, J. B. Klauda, Update of the cholesterol force field parameters in CHARMM, J. Phys. Chem. B 116 (1) (2012) 203–210.

[112] J. P. M. Jämbeck, A. P. Lyubartsev, Implicit inclusion of atomic polarization in modeling of partitioning between water and lipid bilayers, Phys. Chem. Chem. Phys. 15 (2013) 4677–4686.

[113] B. D. Madej, I. R. Gould, R. C. Walker, A parameterization of cholesterol for mixed lipid bilayer simulation within the Amber Lipid14 force field, J. Phys. Chem. B 119 (38) (2015) 12424–12435.

[114] X. Zhuang, J. R. Makover, W. Im, J. B. Klauda, A systematic molecular dynamics simulation study of temperature dependent bilayer structural properties, Biochim. Biophys. Acta 1838 (10) (2014) 2520 – 2529.

[115] M. Höltje, T. Förster, B. Brandt, T. Engels, W. von Rybinski, H.-D. Höltje, Molecular dynamics simulations of stratum corneum lipid models: fatty acids and cholesterol, Biochim. Biophys. Acta 1511 (2001) 156 – 167.

[116] M. T. Hyvönen, T. T. Rantala, M. Ala-Korpela, Structure and dynamic properties of diunsaturated 1-palmitoyl-2-linoleoyl-sn-glycero-3-phosphatidylcholine lipid bilayer from molecular dynamics simulation, Biophys. J. 73 (1997) 2907–2923.

[117] M. Hyvönen, M. Ala-Korpela, J. Vaara, T. T. Rantala, J. Jokisaari, Inequivalence of single CHa and CHb methylene bonds in the interior of a diunsaturated lipid bilayer from a molecular dynamics simulation, Chem. Phys. Lett. 268 (12) (1997) 55 – 60.

[118] S. Feller, D. Yin, R. Pastor, A. M. Jr, Molecular dynamics simulation of unsaturated lipid bilayers at low hydration: parameterization and comparison with diffraction studies, Biophys. J. 73 (5) (1997) 2269 – 2279.

[119] L. Saiz, M. L. Klein, Structural properties of a highly polyunsaturated lipid bilayer from molecular dynamics simulations, Biophys. J. 204 (2001) 204–216.

[120] T. Huber, K. Rajamoorthi, V. F. Kurze, K. Beyer, M. F. Brown, Structure of docosahexaenoic acid-containing phospholipid bilayers as studied by ^{2}H NMR and molecular dynamics simulations, J. Am. Chem. Soc. 124 (2002) 298–309.

[121] S. E. Feller, K. Gawrisch, A. D. MacKerell Jr., Polyunsaturated fatty acids in lipid bilayers: Intrinsic and environmental contributions to their unique physical properties, J. Am. Chem. Soc. 124 (2002) 318–326.

[122] T. Róg, K. Murzyn, R. Gurbiel, Y. Takaoka, A. Kusumi, M. Pasenkiewicz-Gierula, Effects of phospholipid unsaturation on the bilayer nonpolar region: a molecular simulation study, J. lipid Res. 45 (2) (2004) 326–336.

[123] M. T. Hyvönen, P. T. Kovanen, Molecular dynamics simulations of unsaturated lipid bilayers: Effects of varying number of double bonds., Eur. Biophys. J. 34 (2005) 294–305.

[124] J. B. Klauda, V. Monje, T. Kim, W. Im, Improving the CHARMM force field for polyunsaturated fatty acid chains, J. Phys. Chem. B 116 (31) (2012) 9424–9431.

[125] W. Kulig, M. Pasenkiewicz-Gierula, T. Róg, Cis and trans unsaturated phosphatidylcholine bilayers: A molecular dynamics simulation study, Chem. Phys. Lipids 195 (2016) 12 – 20.

[126] H. I. Petrache, S. W. Dodd, M. F. Brown, Area per lipid and acyl length distributions in fluid phosphatidylcholine determined by ^{2}H NMR spectroscopy, Biophys. J. 79 (2000) 3172–3192.

[127] K. Rajamoorthi, M. F. Brown, Bilayers of arachidonic acid containing phospholipids studied by ^{2}H and ^{31}P NMR spectroscopy, Biochemistry 30 (1991) 4204–4212.

[128] H. Schindler, J. Seelig, Deuterium order parameters in relation to thermodynamic properties of a phospholipid bilayer. statistical mechanical interpretation, Biochemistry 14 (11) (1975) 2283–2287.

[129] N. V. Eldho, S. E. Feller, S. Tristram-Nagle, I. V. Polozov, K. Gawrisch, Polyunsaturated docosahexaenoic vs docosapentaeoic acid-differences in lipid matrix properties from the loss of one double bond, J. Am. Chem. Soc. 125 (2003) 6409–6421.

[130] W. Stillwell, S. R. Wassall, Docosahexaenoic acid: Membrane properties of a unique fatty acid, Chem. Phys. Lipids 126 (2003) 1–27.

[131] K. Gawrisch, N. V. Eldho, L. L. Holte, The structure of DHA in phospholipid membranes, Lipids 38 (2003) 445–452.

[132] J. H. Ipsen, G. Karlström, O. Mourtisen, H. Wennerström, M. Zuckermann, Phase equilibria in the phosphatidylcholine-cholesterol system, Biochim. Biophys. Acta 905 (1) (1987) 162 – 172.

[133] T. Róg, M. Pasenkiewicz-Gierula, I. Vattulainen, M. Karttunen, Ordering effects of cholesterol and its analogues, Biochim. Biophys. Acta 1788 (2009) 97 – 121.

[134] P. Somerharju, J. A. Virtanen, K. H. Cheng, M. Hermansson, The superlattice model of lateral organization of membranes and its implications on membrane

lipid homeostasis, Biochim. Biophys. Acta - Biomembranes 1788 (2009) 12 – 23.

[135] T. Róg, I. Vattulainen, Cholesterol, sphingolipids, and glycolipids: What do we know about their role in raft-like membranes?, Chem. Phys. Lipids 184 (2014) 82 – 104.

[136] A. J. Sodt, M. L. Sandar, K. Gawrisch, R. W. Pastor, E. Lyman, The molecular structure of the liquid-ordered phase of lipid bilayers, J. Am. Chem. Soc. 136 (2) (2014) 725–732.

[137] K. Gawrisch, D. Ruston, J. Zimmerberg, V. Parsegian, R. Rand, N. Fuller, Membrane dipole potentials, hydration forces, and the ordering of water at membrane surfaces, Biophys. J. 61 (5) (1992) 1213 – 1223.

[138] H. Akutsu, T. Nagamori, Conformational analysis of the polar head group in phosphatidylcholine bilayers: a structural change induced by cations, Biochemistry 30 (1991) 4510–4516.

[139] D. J. Semchyschyn, P. M. Macdonald, Conformational response of the phosphatidylcholine headgroup to bilayer surface charge: torsion angle constraints from dipolar and quadrupolar couplings in bicelles, Magn. Res. Chem. 42 (2) (2004) 89–104.

[140] A. Arkhipov, Y. Shan, R. Das, N. Endres, M. Eastwood, D. Wemmer, J. Kuriyan, D. Shaw, Architecture and membrane interactions of the EGF receptor, Cell 152 (3) (2013) 557 – 569.

[141] K. Kaszuba, M. Grzybek, A. Orlowski, R. Danne, T. Róg, K. Simons, U. Coskun, I. Vattulainen, N-glycosylation as determinant of epidermal growth factor receptor conformation in membranes, Proc. Natl. Acad. Sci. U.S.A. 112 (2015) 4334–4339.

[142] R. Harris, Nuclear magnetic resonance spectroscopy, John Wiley and Sons Inc.,New York, NY, 1986.

[143] B. Halle, H. Wennerström, Interpretation of magnetic resonance data from water nuclei in heterogeneous systems, J. Chem. Phys. 75 (1981) 1928–1943.

[144] A. Nowacka, P. C. Mohr, J. Norrman, R. W. Martin, D. Topgaard, Polarization transfer solid-state NMR for studying surfactant phase behavior, Langmuir 26 (22) (2010) 16848–16856.

[145] G. Lipari, A. Szabo, Model-free approach to the interpretation of nuclear magnetic resonance relaxation in macromolecules. 1. theory and range of validity, J. Am. Chem. Soc. 104 (17) (1982) 4546–4559.

[146] M. F. Roberts, A. G. Redfield, High-resolution ^{31}P field cycling NMR as a probe of phospholipid dynamics, J. Am. Chem. Soc. 126 (2004) 13765–13777.

[147] M. F. Roberts, A. G. Redfield, Phospholipid bilayer surface configuration probed quantitatively by ^{31}P field-cycling NMR, Proc. Natl. Acad. Sci. U.S.A. 101 (49) (2004) 17066–17071.

[148] M. F. Roberts, A. G. Redfield, U. Mohanty, Phospholipid reorientation at the lipid/water interface measured by high resolution ^{31}P field cycling NMR spectroscopy, Biophys. J. 97 (2009) 132 – 141.

[149] E. Lindahl, O. Edholm, Molecular dynamics simulation of NMR relaxation rates and slow dynamics in lipid bilayers, J. Chem. Phys. 115 (2001) 4938–4950.

[150] J. Wohlert, O. Edholm, Dynamics in atomistic simulations of phospholipid membranes: Nuclear magnetic resonance relaxation rates and lateral diffusion, J. Chem. Phys. 125 (20).

[151] M. Abraham, D. van der Spoel, E. Lindahl, B. Hess, the GROMACS development team, GROMACS user manual version 5.0.7 (2015).
URL `www.gromacs.org`

[152] R. Venable, Y. Zhang, B. Hardy, R. Pastor, Molecular dynamics simulations of a lipid bilayer and of hexadecane: an investigation of membrane fluidity, Science 262 (5131) (1993) 223–226.

[153] R. W. Pastor, R. M. Venable, S. E. Feller, Lipid bilayers, NMR relaxation, and computer simulations, Acc. Chem. Res. 35 (2002) 438–446.

[154] O. Edholm, Time and length scales in lipid bilayer simulations, in: S. E. Feller (Ed.), Computational Modeling of Membrane Bilayers, Vol. 60 of Current Topics in Membranes, Academic Press, 2008, pp. 91 – 110.

[155] J. B. Klauda, N. V. Eldho, , K. Gawrisch, B. R. Brooks, , R. W. Pastor, Collective and noncollective models of NMR relaxation in lipid vesicles and multilayers, J. Phys. Chem. B 112 (2008) 5924–5929.

[156] J. B. Klauda, M. F. Roberts, A. G. Redfield, B. R. Brooks, R. W. Pastor, Rotation of lipids in membranes: Molecular dynamics simulation, ^{31}P spin-lattice relaxation, and rigid-body dynamics, Biophys. J. 94 (8) (2008) 3074 – 3083.

[157] S. E. Feller, D. Huster, K. Gawrisch, Interpretation of NOESY cross-relaxation rates from molecular dynamics simulation of a lipid bilayer, J. Am. Chem. Soc. 121 (1999) 8963–8964.

[158] M. F. Brown, A. A. Ribeiro, G. D. Williams, New view of lipid bilayer dynamics from ^{2}H and ^{13}C NMR relaxation time measurements, Proc. Natl. Acad. Sci. U.S.A. 80 (14) (1983) 4325–4329.

[159] T. M. Ferreira, Structure and dynamics in amphiphilic bilayers: NMR and MD simulation studies, Ph.D. thesis, Lund University, http://lup.lub.lu.se/record/3878850/file/3879121.pdf (2013).

[160] Y. Lyatskaya, Y. Liu, S. Tristram-Nagle, J. Katsaras, J. F. Nagle, Method for obtaining structure and interactions from oriented lipid bilayers, Phys Rev E 63 (2001) 11907.

[161] N. Kučerka, Y. Liu, N. Chu, H. I. Petrache, S. Tristram-Nagle, J. F. Nagle, Structure of fully hydrated fluid phase DMPC and DLPC lipid bilayers using X-ray scattering from oriented multilamellar arrays and from unilamellar vesicles, Biophys. J. 88 (2005) 2626 – 2637.

[162] P. Heftberger, B. Kollmitzer, F. A. Heberle, J. Pan, M. Rappolt, H. Amenitsch, N. Kučerka, J. Katsaras, G. Pabst, Global small-angle x-ray scattering data analysis for multilamellar vesicles: the evolution of the scattering density profile model, J. Appl. Crystallogr. 47 (2014) 173–180.

[163] R. Zhang, R. M. Suter, J. F. Nagle, Theory of the structure factor of lipid bilayers, Phys Rev E 50 (1994) 5047–5059.

[164] N. Kučerka, S. Tristam-Nagle, J. F. Nagle, Structure of fully hydrated fluid phase lipid bilayers with monounsaturated chains, J. Membrane Biol. 208 (2005) 193–202.

[165] N. Kučerka, J. Pencer, J. N. Sachs, J. F. Nagle, J. Katsaras, Curvature effect on the structure of phospholipid bilayers, Langmuir 23 (3) (2007) 1292–1299.

[166] G. Büldt, H. Gally, A. seelig, J. Seelig, G. Zaccai, Neutron diffraction studies on selectively deuterated phospholipid bilayers, Nature 271 (1978) 182–184.

[167] G. Büldt, H. Gally, J. Seelig, G. Zaccai, Neutron diffraction studies on phosphatidylcholine model membranes, J. Mol. Biol. 134 (4) (1979) 673 – 691.

[168] L. Herbette, C. Napolitano, R. McDaniel, Direct determination of the calcium profile structure for dipalmitoyllecithin multilayers using neutron diffraction, Biophys. J. 46 (6) (1984) 677 – 685.

[169] N. Kučerka, J. F. Nagle, J. N. Sachs, S. E. Feller, J. Pencer, A. Jackson, J. Katsaras, Lipid bilayer structure determined by the simultaneous analysis of neutron and x-ray scattering data, Biophys. J. 95 (2008) 2356 – 2367.

[170] V. F. Sears, Neutron scattering lengths and cross sections, Neutron News 3 (3) (1992) 26–37.

[171] R. W. Benz, F. Castro-Romn, D. J. Tobias, S. H. White, Experimental validation of molecular dynamics simulations of lipid bilayers: A new approach, Biophys. J. 88 (2) (2005) 805 – 817.

[172] D. T. Cromer, J. B. Mann, X-ray scattering factors computed from numerical hartreefock wave functions, Acta Crystallogr. A 24 (1968) 321–324.

[173] A. Braun, E. Brandt, O. Edholm, J. Nagle, J. Sachs, Determination of electron density profiles and area from simulations of undulating membranes, Biophys. J. 100 (9) (2011) 2112 – 2120.

[174] J. Pan, S. Tristram-Nagle, J. F. Nagle, Effect of cholesterol on structural and mechanical properties of membranes depends on lipid chain saturation, Phys. Rev. E 80 (2) (2009) 021931.

[175] N. Kučerka, J. Pencer, M.-P. Nieh, J. Katsaras, Influence of cholesterol on the bilayer properties of monounsaturated phosphatidylcholine unilamellar vesicles, Eur. Phys. J. E 23 (3) (2007) 247–254.

[176] J. Pan, T. T. Mills, S. Tristram-Nagle, J. F. Nagle, Cholesterol perturbs lipid bilayers nonuniversally, Phys. Rev. Lett. 100 (19) (2008) 198103.

[177] A. Hodzic, M. Rappolt, H. Amenitsch, P. Laggner, G. Pabst, Differential modulation of membrane structure and fluctuations by plant sterols and cholesterol, Biophys. J. 94 (10) (2008) 3935 – 3944.

[178] G. Khelashvili, G. Pabst, D. Harries, Cholesterol orientation and tilt modulus in dmpc bilayers, J. Phys. Chem. B 114 (22) (2010) 7524–7534.

[179] T. A. Harroun, J. Katsaras, S. R. Wassall, Cholesterol is found to reside in the center of a polyunsaturated lipid membrane, Biochemistry 47 (27) (2008) 7090–7096.

[180] S. J. Marrink, A. H. de Vries, T. A. Harroun, J. Katsaras, , S. R. Wassall, Cholesterol shows preference for the interior of polyunsaturated lipid membranes, J. Am. Chem. Soc. 130 (1) (2008) 10–11.

[181] N. Kučerka, D. Marquardt, T. A. Harroun, M.-P. Nieh, S. R. Wassall, D. H. de Jong, L. V. Schäfer, S. J. Marrink, J. Katsaras, Cholesterol in bilayers with

PUFA chains: Doping with DMPC or POPC results in sterol reorientation and membrane-domain formation, Biochemistry 49 (2010) 7485–7493.

[182] F. Heberle, J. Pan, R. Standaert, P. Drazba, N. Kučerka, J. Katsaras, Model-based approaches for the determination of lipid bilayer structure from small-angle neutron and x-ray scattering data, Eur. Biophys. J. 41 (10) (2012) 875–890.

[183] J. C. Fogarty, M. Arjunwadkar, S. A. Pandit, J. Pan, Atomically detailed lipid bilayer models for the interpretation of small angle neutron and x-ray scattering data, Biochim. Biophys. Acta 1848 (2) (2015) 662 – 672.

[184] J. N. Sachs, H. I. Petrache, T. B. Woolf, Interpretation of small angle x-ray measurements guided by molecular dynamics simulations of lipid bilayers, Chem. Phys. Lipids 126 (2) (2003) 211 – 223.

[185] J. B. Klauda, N. Kuerka, B. R. Brooks, R. W. Pastor, J. F. Nagle, Simulation-based methods for interpreting x-ray data from lipid bilayers, Biophys. J. 90 (8) (2006) 2796 – 2807.

[186] N. Kučerka, J. D. Perlmutter, J. Pan, S. Tristram-Nagle, J. Katsaras, J. N. Sachs, The effect of cholesterol on short- and long-chain monounsaturated lipid bilayers as determined by molecular dynamics simulations and x-ray scattering, Biophys. J. 95 (6) (2008) 2792 – 2805.

[187] A. R. Braun, J. N. Sachs, J. F. Nagle, Comparing simulations of lipid bilayers to scattering data: The GROMOS 43A1-S3 force field, J. Phys. Chem. B 117 (17) (2013) 5065–5072.

[188] P. Heftberger, B. Kollmitzer, A. Rieder, H. Amenitsch, G. Pabst, In situ determination of structure and fluctuations of coexisting fluid membrane domains, Biophys. J. 108 (4) (2015) 854 – 862.

[189] Q. D. Pham, D. Topgaard, E. Sparr, Cyclic and linear monoterpenes in phospholipid membranes: Phase behavior, bilayer structure, and molecular dynamics, Langmuir 31 (40) (2015) 11067–11077.

[190] S. K. Hansen, K. Bertelsen, B. Paaske, N. C. Nielsen, T. Vosegaard, Solid-state NMR methods for oriented membrane proteins, Prog. Nucl. Magn. Reson. Spectrosc. 8889 (2015) 48 – 85.

[191] A. Spaar, T. Salditt, Short range order of hydrocarbon chains in fluid phospholipid bilayers studied by x-ray diffraction from highly oriented membranes, Biophys. J. 85 (3) (2003) 1576–1584.

[192] R. B. Best, J. Mittal, Free-energy landscape of the GB1 hairpin in all-atom explicit solvent simulations with different force fields: Similarities and differences, Proteins: Struct. Funct. Bioinf. 79 (4) (2011) 1318–1328.

[193] K. A. Beauchamp, Y.-S. Lin, R. Das, V. S. Pande, Are protein force fields getting better? a systematic benchmark on 524 diverse NMR measurements, J. Chem. Theory Comput. 8 (4) (2012) 1409–1414.

[194] S. Rauscher, V. Gapsys, M. J. Gajda, M. Zweckstetter, B. L. de Groot, H. Grubmüller, Structural ensembles of intrinsically disordered proteins depend strongly on force field: A comparison to experiment, J. Chem. Theory Comput. 11 (11) (2015) 5513–5524.